ARTICLE



Textural characteristics of ore mineral dendrites in banded quartz veins from low-sulfidation epithermal deposits: implications for the formation of bonanza-type precious metal enrichment

Erik R. Tharalson¹ • Tadsuda Taksavasu¹ • Thomas Monecke¹ • T. James Reynolds^{1,2} • Nigel M. Kelly^{1,3} • Katharina Pfaff¹ • Aaron S. Bell⁴ • Ross Sherlock⁵

Received: 24 May 2021 / Accepted: 12 June 2023 © The Author(s), under exclusive licence to Springer-Verlag GmbH Germany, part of Springer Nature 2023

Abstract

Quartz veins in bonanza-type ore zones of low-sulfidation epithermal deposits frequently contain ore mineral dendrites. Gold and naumannite dendrites hosted by colloform silica bands from four deposits located in California and Nevada were studied to better understand the processes by which these delicate ore mineral aggregates are formed. High-magnification optical petrography revealed that the colloform bands hosting the ore mineral dendrites originally consisted of non-crystalline silica microspheres. Textural relationships suggest that the microspherical silica provided the structural framework for the delicate ore mineral aggregates to grow. The ore mineral dendrites either grew contemporaneously with the deposition of the microspherical silica along the vein walls or after their deposition within permeable gel-like layers of microspheres. Etching in hydrofluoric acid showed that the ore mineral dendrites exhibit complex surface morphologies. The surface morphology of the ore mineral dendrites and their textural relationships with the silica host were modified as a result of post-depositional maturation and recrystallization causing the conversion of the non-crystalline silica to quartz. It is proposed here that ore mineral dendrites formed in low-sulfidation epithermal veins during periods of two-phase flow associated with short-lived events of vigorous boiling or flashing, which caused supersaturation of silica in the liquid and the deposition of the ore minerals.

Keywords Low-sulfidation epithermal · Gold · Silver · Dendrites · Bonanza grade · Flashing

Editorial handling: M. Steele-Macinnis

Erik R. Tharalson etharals@mines.edu

Published online: 04 July 2023

- Center to Advance the Science of Exploration to Reclamation in Mining, Department of Geology and Geological Engineering, Colorado School of Mines, 1516 Illinois Street, Golden, CO 80401, USA
- FLUID INC., 1401 Wewatta St. #PH3, Denver, CO 80202, USA
- Bruker Nano Analytics, Madison, WI 53711, USA
- Department of Geological Sciences, University of Colorado Boulder, 2200 Colorado Avenue, Boulder, CO 80309, USA
- Mineral Exploration Research Centre, Harquail School of Earth Sciences, Laurentian University, 935 Ramsey Lake Road, Sudbury, ON P3E 2C6, Canada

Introduction

Low-sulfidation epithermal deposits form in the shallow subsurface (< 1.5 km) from near-neutral hydrothermal waters having temperatures of up to ~250 °C (Hedenquist et al. 2000; Simmons et al. 2005). The ore-forming hydrothermal liquids are rock-buffered and typically have a low (< 3–4 wt% NaCl equiv.) salinity (Hedenquist et al. 2000; Bodnar et al. 2014). Many low-sulfidation epithermal deposits have zones of bonanza-type ore grades confined to crustiform quartz veins that range from centimeters to several meters in width. Within these crustiform veins, the ore minerals typically occur within specific colloform bands (Takeuchi and Shikazono 1984; Leavitt et al. 2004; Sanematsu et al. 2006; Shimizu 2014; Tharalson et al. 2019).

The ore minerals within crustiform quartz veins in lowsulfidation epithermal deposits commonly have complex dendritic shapes. In some deposits, macroscopic ore mineral dendrites occur. Large gold dendrites in bonanza-type ore zones include those at the Jumbo, Fire Creek, Midas,



National, Round Mountain, Seven Troughs, Sleeper, and Tenmile deposits in Nevada (Lindgren 1915; Saunders 1990, 1994, 2012; Saunders and Schoenly 1995a; Saunders et al. 1996, 2020; Perez 2013; Milliard et al. 2015; Burke et al. 2017; Saunders and Burke 2017); McLaughlin in California (Sherlock and Lehrman 1995); and Khan Krum in Bulgaria (Marinova et al. 2014). Acanthite, aguilarite, and naumannite dendrites have been described from the DeLamar Mountain and War Eagle Mountain deposits in Idaho (Mason et al. 2015) and the Buckskin National, Hollister, Fire Creek, and Seven Troughs deposits in Nevada (Vikre 1985, 2007; Saunders et al. 2008, 2011, 2020; Unger 2008; Saunders 2012). In some deposits, base metal sulfides also form dendrites in crustiform quartz veins. For instance, chalcopyrite encrusting and replacing naumannite has been documented at Buckskin National (Saunders 2012). At the Waihi and Karangahake in New Zealand, sphalerite is fine-grained to dendritic (Simpson 2017). Dendritic galena has been recorded at the Koryu deposit in Japan (Shimizu et al. 1998).

The processes involved in the formation of ore mineral dendrites in the crustiform quartz veins of low-sulfidation epithermal deposits are currently not fully understood. Early workers, including Lindgren (1936), suggested that the formation of gold dendrites can be linked to colloidal gold transport in the hydrothermal liquids. This model was further refined by Saunders (1990), Saunders and Schoenly (1995a,b), as well as Sherlock and Lehrman (1995). Saunders (1990) suggested that gold forms colloids in the deeper parts of the hydrothermal system as a result of cooling or boiling of the hydrothermal liquids. In this model, colloidal gold would then have been mechanically transported by the hydraulic action of the ore-forming hydrothermal liquid and grown through aggregation. The nanoparticles of gold would have deposited along the vein walls through density accumulation or scavenging by charged surfaces. Ultimately, upward growth of the gold dendrites would have occurred at the tips of the dendrite branches simultaneously to the deposition of the silica host along the vein walls, successively building up a silica layer that hosts large dendrites. Saunders et al. (2011) suggested that colloidal transport is not restricted to gold and that naumannite dendrites may have formed by a similar process. Nevertheless, the textural relationships between the ore mineral dendrites and the colloform bands have not been described in detail, and the question as to why adjacent colloform bands in these crustiform veins commonly show different ore mineralogy (Taksavasu et al. 2018; Tharalson et al. 2019; Zeeck et al. 2021) has not been fully addressed yet.

To better constrain the processes by which ore mineral dendrites form in crustiform quartz veins in shallow hydrothermal systems, vein material from four low-sulfidation epithermal deposits was selected for this study. The distribution of ore minerals in the crustiform veins and chemical zoning of the ore mineral dendrites was studied by micro X-ray fluorescence (µXRF) mapping. The microtextural characteristics of ore mineral dendrites and their textural relationships to the silica host were identified by optical microscopy. In addition to the study of textural relationships in thin sections, the morphologies of ore mineral dendrites were determined by scanning electron microscopy following etching of samples in concentrated HF. Based on the textural observations, it is suggested that the colloform bands hosting the ore mineral dendrites originally contained non-crystalline microspherical silica. Ore mineral dendrites either grew during stacking of the silica microspheres or grew within the originally permeable, gel-like layers of microspheres deposited along the vein walls during short periods of vigorous boiling or flashing of the hydrothermal liquids. The new model of dendrite growth has significant implications to the current understanding of how bonanza-type precious metal enrichment can develop in crustiform quartz veins in low-sulfidation epithermal systems.

Geological setting

Vein samples containing ore mineral dendrites were obtained from four low-sulfidation epithermal deposits located in the Western United States (Fig. 1). This included gold dendrites from McLaughlin in California and Sleeper in Nevada as well as naumannite dendrites from the Buckskin National and Fire Creek deposits in Nevada.

The Pleistocene (<2.2 Ma) McLaughlin deposit is located in the Coast Ranges of California, ~ 120 km north of San Francisco (Gustafson 1991). McLaughlin is a well-preserved low-sulfidation epithermal deposit that underwent little erosion since its formation as the mineralized vein system is capped by hydrothermal eruption deposits and a subaerial sinter terrace. Mineralization is located in the structural footwall of the Stony Creek fault separating the Middle Jurassic Coast Range ophiolite in the southwest from Late Jurassic sedimentary rocks of the Great Valley sequence to the northeast (Sherlock et al. 1995; Tosdal et al. 1996). Highgrade ores occur in a pipe-like sheeted vein complex that developed within a dilatant zone at the margin of a basalt block within a tectonic mélange consisting of sedimentary rocks and serpentinite. The sheeted vein complex consists of centimeter- to meter-wide subparallel siliceous veins (Sherlock and Lehrman 1995; Sherlock et al. 1995; Tosdal et al. 1996). The deposit was mined between 1983 and 1996, with a total resource of ~3.5 million ounces (Moz) Au contained in 24.3 million metric tonnes (Mt) of ore grading 4.49 g/t (Tosdal et al. 1996).

The Sleeper deposit is located at the western flank of the Slumbering Hills of Humboldt County, Nevada, ~45 km northwest of Winnemucca (Wood and Hamilton 1991).



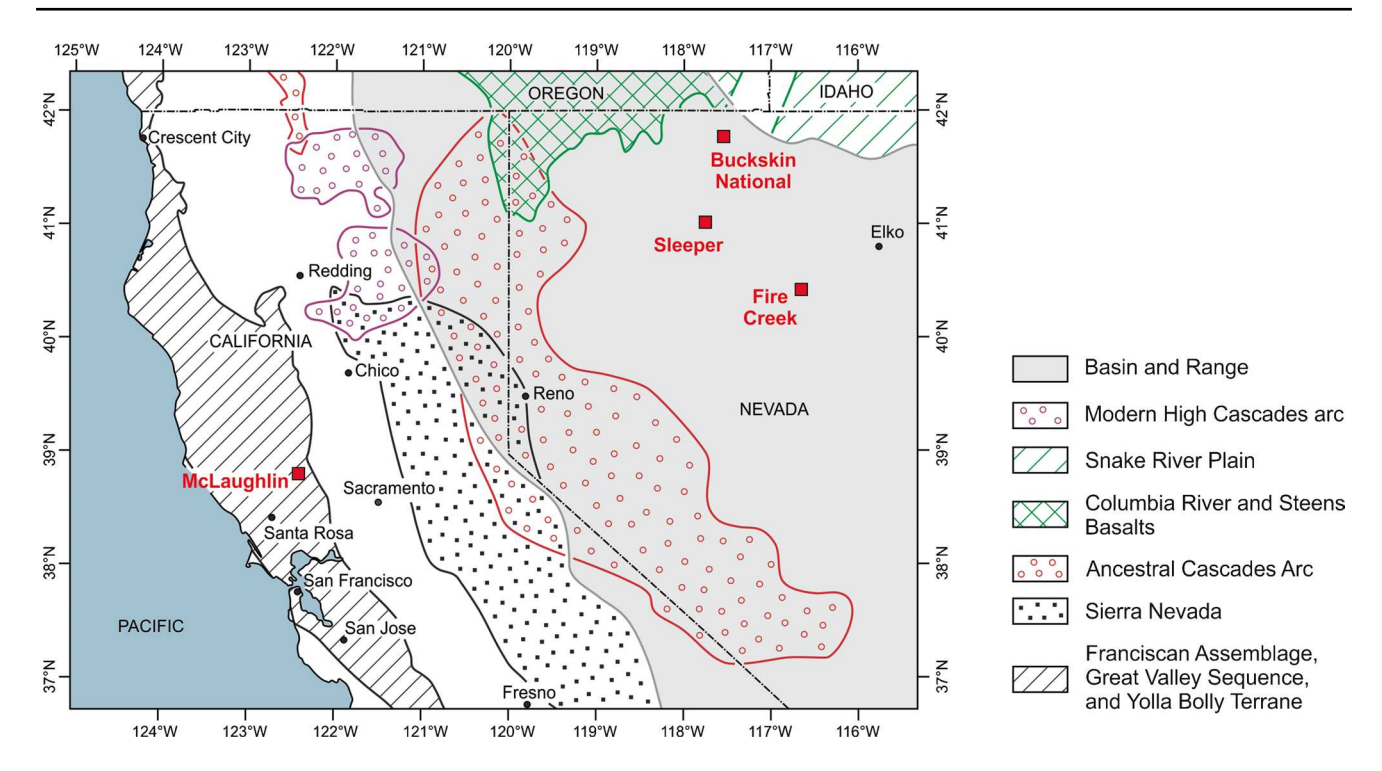


Fig. 1 Map showing the locations of the low-sulfidation epithermal deposits studied. Major geological units modified from John and Henry (2020)

Sleeper is hosted by early Miocene volcanic rocks which were deposited on folded Mesozoic metasedimentary basement rocks. The volcanic succession includes a < 40-200-m-thick basal volcaniclastic unit that is overlain by a 150-m-thick unit of basaltic to andesitic flows and associated breccias. A pumiceous lapilli tuff unit separates the basaltic to andesitic flows from an overlying, over 300-m-thick porphyritic rhyolite unit that is the main host to gold mineralization at Sleeper (Nash et al. 1995). Bonanzatype veins are crustiform and range from 2 cm to 5 m in width, with typical grades of 50-100 g/t Au. The veins occur in a zone that is 300 m wide and 1200 m in strike length. Four continuous high-grade veins have been identified that each can be traced over a strike length of ~200 m each, with a down-dip extent of over 300 m. These bonanza-type veins are surrounded by narrow (<5 m) breccia zones, typically grading 3-35 g/t Au, that grade outward into brecciated wall rock cut by stockwork veins, with low gold grades extending up to 200 m in the structural hanging wall of the veins (Nash et al. 1989, 1995). ⁴⁰Ar/³⁹Ar dating of adularia from Sleeper suggests that the mineralization formed between 16.2 ± 0.4 and 14.1 ± 0.6 Ma (Conrad et al. 1993). Mining of the deposit between 1986 and 1996 produced ~ 1.7 Moz Au and ~2.3 Moz Ag (Wilson and Brechtel 2017).

The Buckskin National deposit forms part of the National district of Humboldt County, Nevada (Lindgren 1915; Vikre 1985, 1987, 2007). The deposit was mined

intermittently from 1906 to 1941, yielding 24,000 oz Au and 300,000 oz Ag. The Buckskin National deposit is hosted by a ~ 700-m-thick succession of early Miocene (16.57 ± 0.03) to 16.11 ± 0.03 Ma; Vikre 2007) massive rhyolite and associated volcaniclastic rocks. The mine was developed on a bonanza-type vein referred to as the Bell vein. Mining of the Bell vein has occurred over a strike length of 1.3 km. The vein strikes N-S and dips 75° to the west. It has an average thickness of 1.8 m (Vikre 1985). Based on drilling, the vein is known to extend to a depth of at least ~ 790 m below the paleosurface (Vikre 2007). The Bell vein consists primarily of quartz with adularia being the second most abundant gangue mineral. ⁴⁰Ar/³⁹Ar dating of adularia yielded an age of 16.06 ± 0.03 Ma (Vikre 2007). The top of Buckskin Mountain is capped by a 30-m-thick carapace of finely laminated silica sinter and silicified epiclastic deposits. The reddish to gray-black silica sinter cropping out in an area that is 420×230 m represents the surface expression of the hydrothermal system that formed the Buckskin National deposit (Vikre 2007).

The Fire Creek deposit is located in the Argenta mining district in Lander County, Nevada, ~100 km west of Elko. The basement in the area is composed of lower Paleozoic siliciclastic rocks that are complexly deformed. These rocks are unconformably overlain by basal conglomerate, and Eocene crystal-rich rhyolite ash-flow tuff that is moderately to densely welded. The rhyolite tuff is overlain by

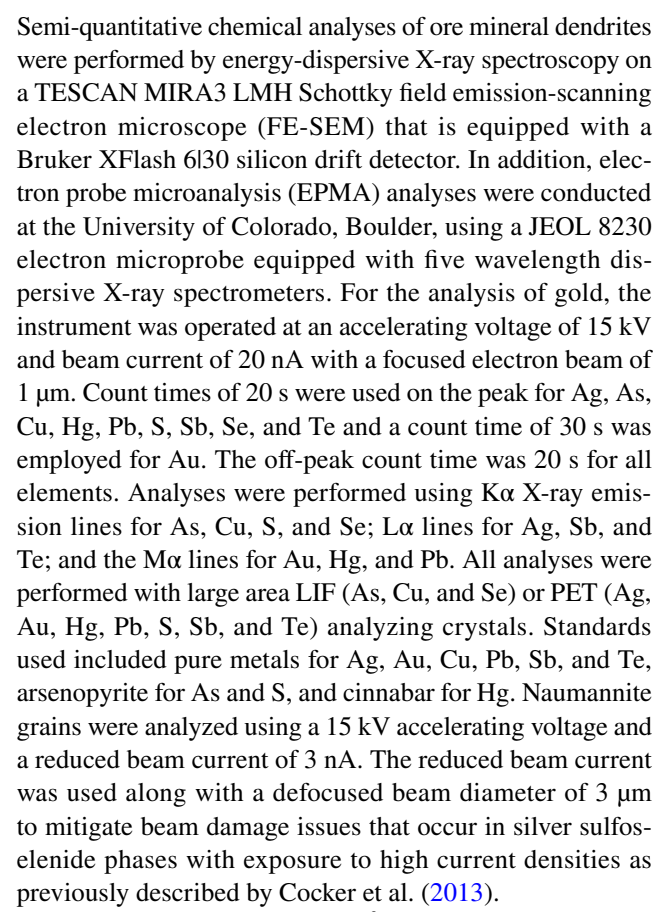


a~150-m-thick Oligocene to Miocene succession of tuffs, basalt to andesite sills, dikes, rare lava flows, lacustrine deposits, and rare epiclastic tuffs. Miocene porphyritic basaltic andesite to andesite flows and associated volcaniclastic rocks form the main host to mineralization at Fire Creek. Lava flows in this 120–220-m-thick unit are marked by distinctive, multi-directional hackly jointing. The lava is overlain by tan to buff colored tuff and lapilli tuff that is locally intruded by vitreous aphanitic basalt sills. A ~ 200-m-thick succession of andesite flows cap the volcanic succession at Fire Creek (Milliard et al. 2015; Odell et al. 2018). Miocene mineralization at the deposit predominately occurs as bonanza-type (up to 30,000 g/t Au) veins developed along faults or dike contacts. The crustiform veins range from < 1 cm to 1.5 m in thickness. In total, over 70 individual veins or mineralized structures have been identified at Fire Creek, forming a mineralized vein array extending for over 1500 m along strike and from near surface to a depth of over 300 m (Perez 2013; Milliard et al. 2015; Odell et al. 2018). In addition to the bonanza-type veins, lower grade breccia zones and disseminated sulfide zones are present in the hackly-jointed basaltic andesite and andesite flows (Milliard et al. 2015). Between 2015 and 2019, Fire Creek produced 385,000 oz Au and 599,000 oz Ag. At the end of 2021, proven and probable reserves of 53,500 metric tonnes of ore grading 31.6 g/t Au and 30.9 g/t Ag were identified, totaling 54,000 oz Au and 51,000 oz Ag. In addition, measured and indicated resources of 121,600 metric tonnes of ore grading 15.8 g/t Au and 34.3 g/t Ag for a total of 61,000 oz Au and 128,000 oz Ag were defined (J. Marma, pers. commun. 2022).

Materials and methods

Initially, chemical mapping of cut hand specimens was performed using a bench-top Bruker M4 Tornado μXRF at the Colorado School of Mines. The instrument is equipped with dual 30 mm² silicon drift detectors and a Rh X-ray tube with polycapillary optics allowing spot sizes of ~25 μm . All measurements were performed under a vacuum of 20 mbar at 50 kV and 600 nA using a 12.5 μm Al primary excitation filter. Data acquisition was conducted at a line spacing of 35 μm and a dwell time of 35 ms per pixel. The X-ray peaks for individual elements were manually checked and used to generate element distribution maps showing normalized count rates using the Bruker M4 ESPRIT software. All element maps were generated using Ka X-ray lines, except Au, where the La line was used.

Polished thin $(35-45 \mu m \text{ thick})$ sections were used to study the dendrite mineralogy and the textural relationships between the ore minerals and the host. Optical petrography was conducted using an Olympus BX51 optical microscope.



Small subsamples (~0.5 cm³) of the crustiform vein material containing ore mineral dendrites were prepared using a micro-saw. These subsamples were etched in 4–5 ml of 48% HF at room temperature without agitation within 15 ml polypropylene tubes for seven days. Subsequently, the samples were decanted and rinsed. The etched ore mineral dendrites were then hand-picked under a binocular microscope and mounted on aluminum sample stubs using carbon tape. Following Au coating, secondary electron imaging of the samples was conducted using a TESCAN MIRA3 LMH Schottky FE-SEM operated at working distances of 5–10 mm and an accelerating voltage of 15.0 kV.

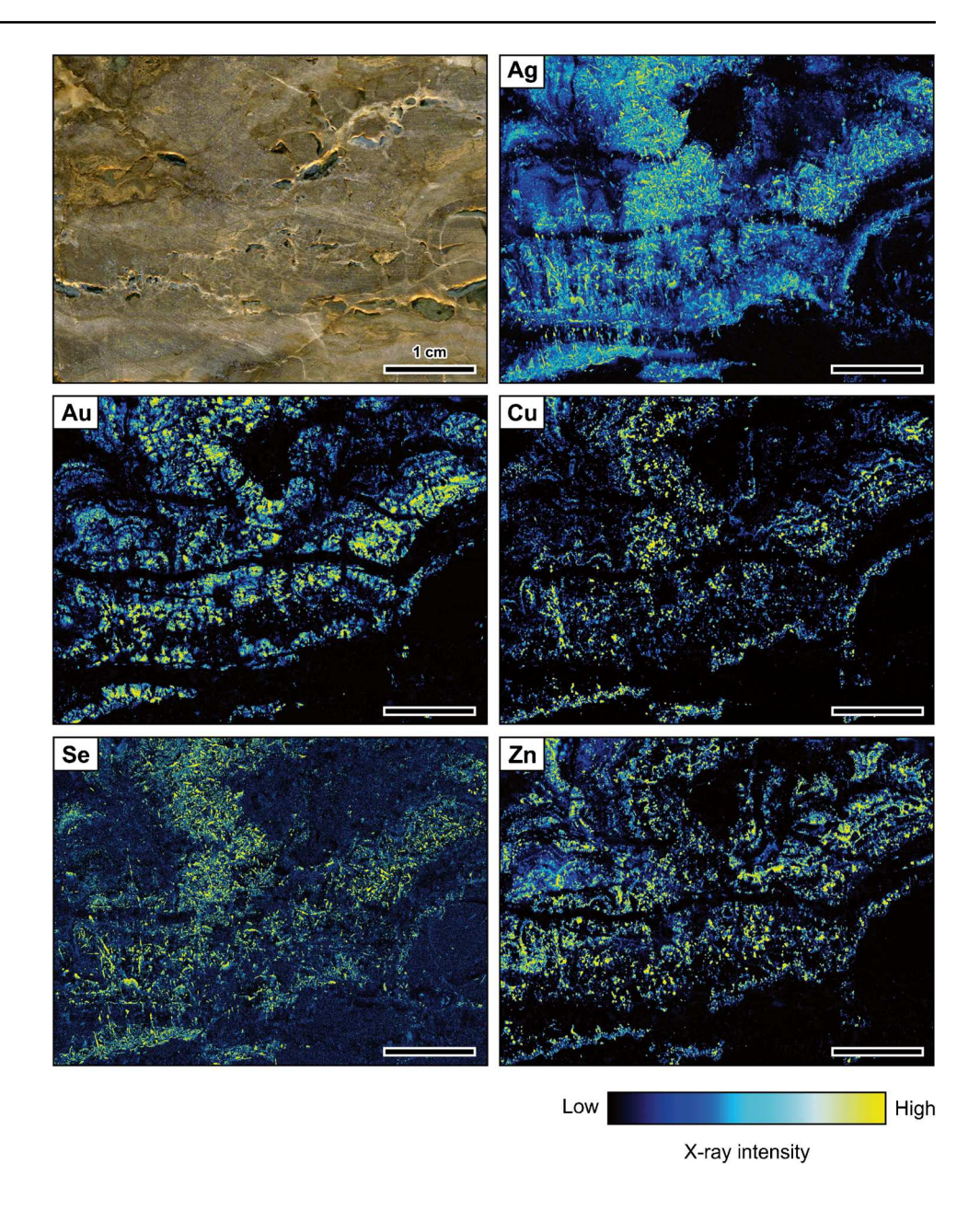
Results

Gold dendrites from McLaughlin

As shown by Sherlock and Lehrman (1995), amber-colored opaline veins occurring within the sheeted vein complex contain abundant gold dendrites that are too small (<0.5 mm) to be visually recognizable (Fig. 2). Chemical mapping by μ XRF shows that elevated Ag and Au count rates occur throughout the vein sample and that macroscopic criteria such as the color of the opaline material is only a poor predictor of where precious metal minerals occur. The



Fig. 2 Sample photograph and corresponding Ag, Au, Cu, Se, and Zn maps of gold dendrites hosted in an ambercolored opaline vein sample from the McLaughlin deposit in California. The dendrites are small (<0.5 mm) and cannot be recognized macroscopically in the opaline host. The element maps were obtained by μXRF



maps show that the distribution of Au is not directly correlated to the distribution of Ag, Cu, Se, and Zn (Fig. 2).

Petrographic investigations of the amber-colored veins show that the opaline material forming these veins consists of tightly packed 1–5 µm relict microspheres (Fig. 3a–d). The relict microspheres can be easily recognized at high magnification (Fig. 3c, d). Cavities between the relict microspheres have sickle-like shapes. The opaline material is colloform banded, with adjacent bands showing subtle differences in color and the packing density of the relict microspheres. The surfaces of individual bands are wavy or botryoidal in shape.

Various degrees of recrystallization of the microspherical silica can be observed. In some of the opaline bands, the relict microspheres are densely packed and appear to be fused together. Groups of concentrically banded silica spheres having a heterogeneous turbid appearance occur (Fig. 3b, e). In plane polarized light, these silica spheres differ in color from the surrounding originally microspherical matrix. Individual spheres are up to 50 µm in size. In many cases, the silica spheres are interconnected, with the outermost concentric bands surrounding entire amalgamated aggregates (Fig. 3b). The microspherical matrix is locally recrystallized to quartz, which can form complex aggregates (Fig. 3b) or doubly terminated quartz crystals (Fig. 3e) that are suspended in the originally microspherical matrix. Where the quartz aggregates or crystals occur in close proximity, the concentric zoning around the crystals resembles colloform banding (Fig. 3e). Dense occurrences of the quartz crystals grown in the originally microspherical matrix locally resulted in the



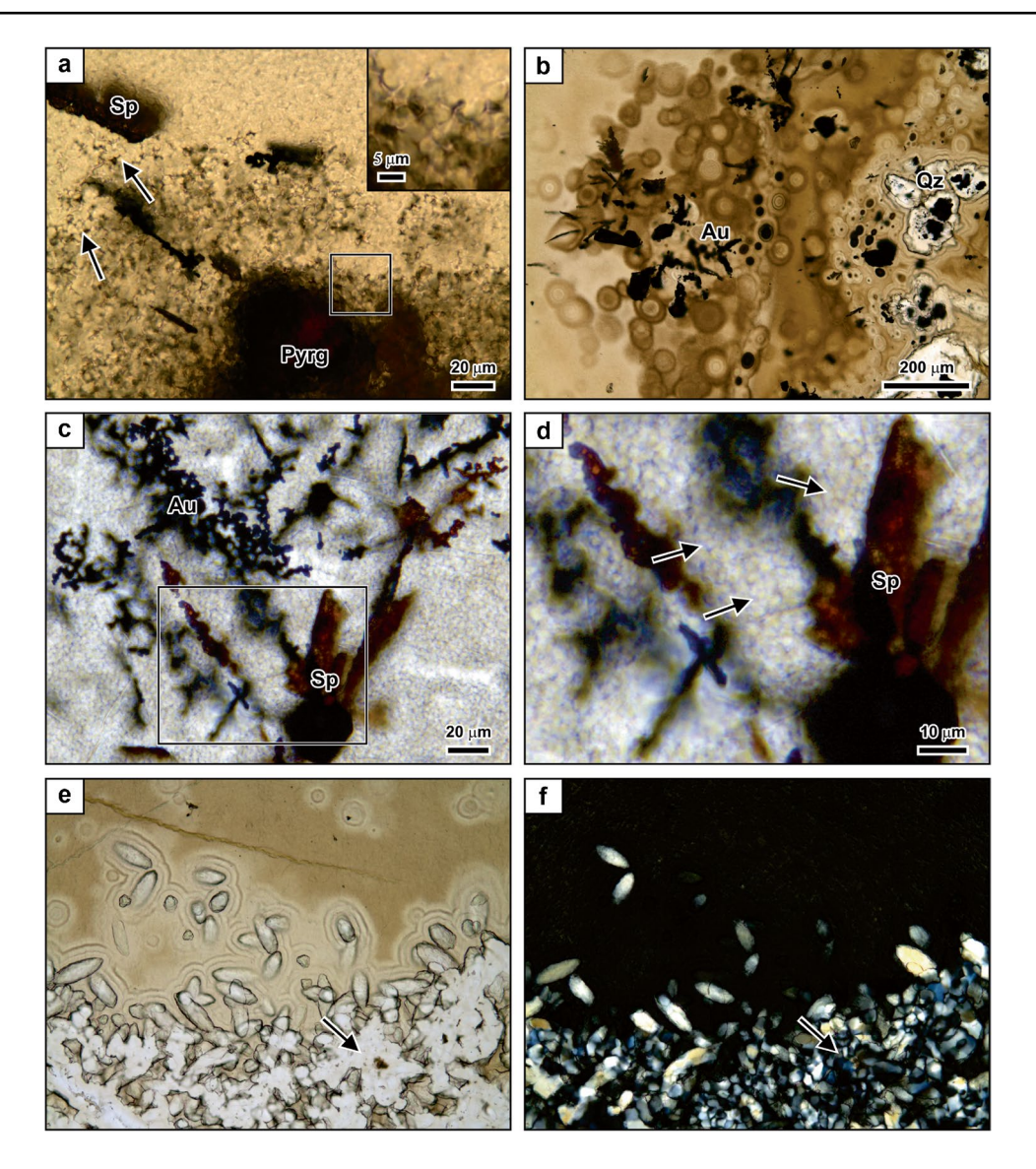


Fig. 3 Photomicrographs of silica textures in opaline vein material from the McLaughlin deposit in California. **a** Ore minerals within a matrix of relict silica microspheres, some of which are highlighted by the arrows. One location with relict microspheres is given as an inset. Plane polarized light. **b** Silica recrystallization textures within a matrix of relict microspheres. Circular and concentric bands surround quartz nucleation sites and quartz crystals with encapsulated ore minerals. Ore minerals are locally encapsulated within crystals of quartz grown in the originally microspherical matrix. Plane polarized light. **c** Originally microspherical silica matrix surrounding gold dendrites and a sphalerite aggregate. The relict silica microspheres are densely

packed. Plane polarized light. **d** High-magnification image of the relict silica microspheres (arrows) shown in the previous image. Plane polarized light. **e** Doubly terminated quartz crystals that have grown within the originally microspherical matrix. Some isolated crystals are surrounded by concentric bands. Dense packing of quartz crystals resulted in the formation of zones of massive clear quartz (arrow). Plane polarized light. **f** Cross-polarized light image of the same field of view. The image shows that the silica matrix is still isotropic. The densely packed quartz crystals exhibit a mosaic texture (arrow). Au gold, *Pyrg* pyrargyrite, *Qz* quartz, *Sp* sphalerite

formation of zones of massive clear quartz crystals (Fig. 3e). In cross-polarized light, these zones exhibit a mosaic texture in which quartz grains have irregular and interpenetrating grain boundaries and differ in their crystallographic orientations (Fig. 3f).

Ore minerals occur throughout the variably recrystallized microspherical matrix (Figs. 3 and 4). Most notable are curviplanar, spinifex-like dendrites, which mostly consist of gold and sphalerite, with minor pyrargyrite, tetrahedrite, and argentite/acanthite (Fig. 4a). These up to 500- μ m-long aggregates are oriented approximately perpendicular to the colloform banding. Ore minerals also occur as small dendrites within the originally microspherical matrix radiating in different directions (Fig. 4b) or show tree-like branching (Fig. 4c). The gold in these dendrites has a millesimal fineness of 593 to 790, averaging 734 (n=70; Fig. 5).



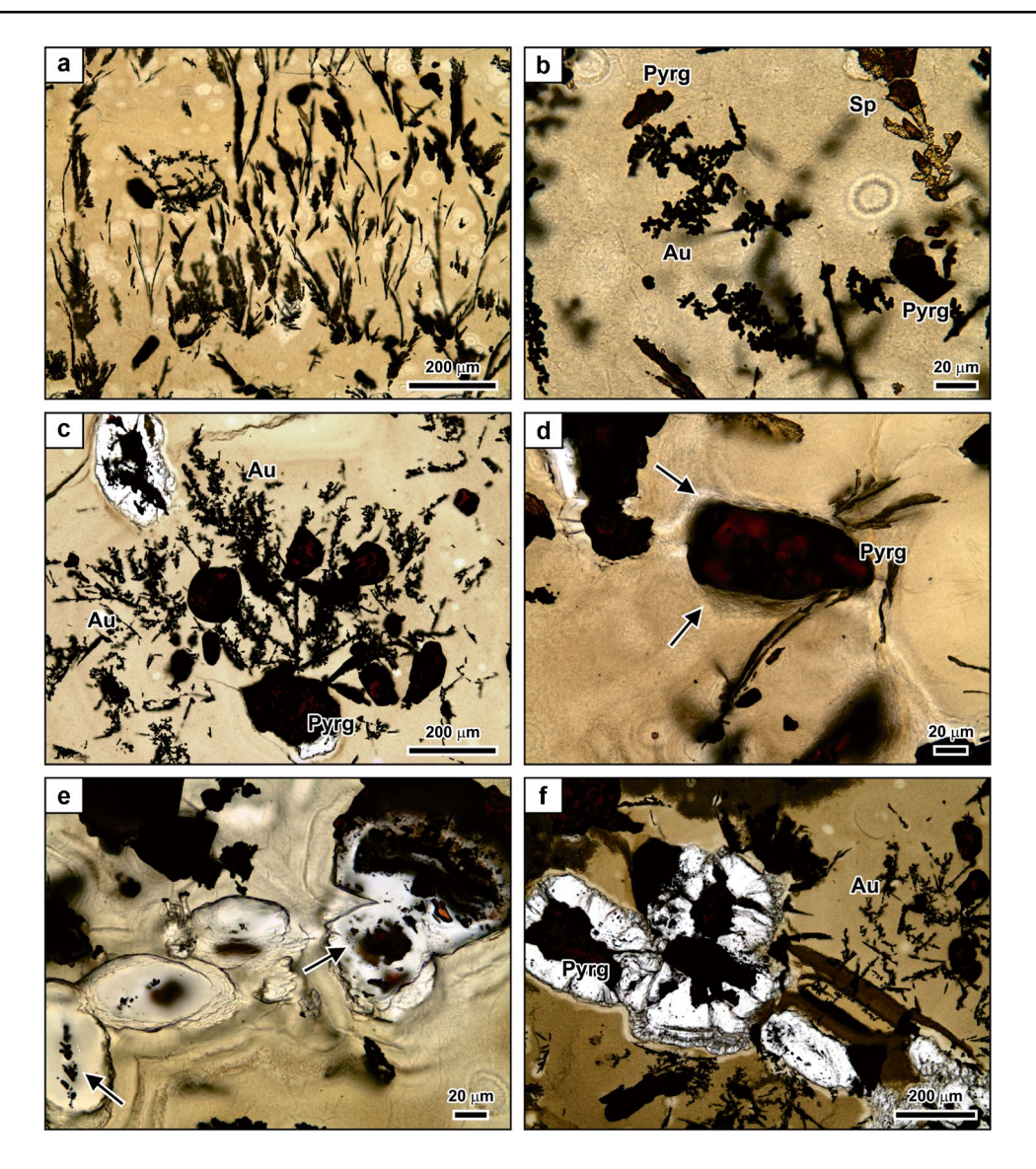


Fig. 4 Photomicrographs of ore mineral textures in opaline vein material from the McLaughlin deposit in California. **a** Curviplanar, spinifex-like dendrite within an originally microspherical silica matrix. The aggregates consist mostly of gold and sphalerite, with minor pyrargyrite and tetrahedrite. These aggregates have grown approximately perpendicular to the vein wall. Circular and concentric banding can be seen within the originally microspherical matrix. **b** High magnification image of gold and sphalerite dendrites suspended in an originally microspherical silica matrix. The larger crystal is pyrargyrite. **c** Delicate gold dendrite grown in an originally microspherical matrix. The dendrite is intergrown with some larger euhedral pyrargyrite grains. A dendritic aggregate in the upper left part of the image is surrounded by clear quartz that is interpreted to have formed through recrystallization of the non-crystalline silica in the matrix. **d** High-magnification image of a large pyrargyrite crystal. The origi-

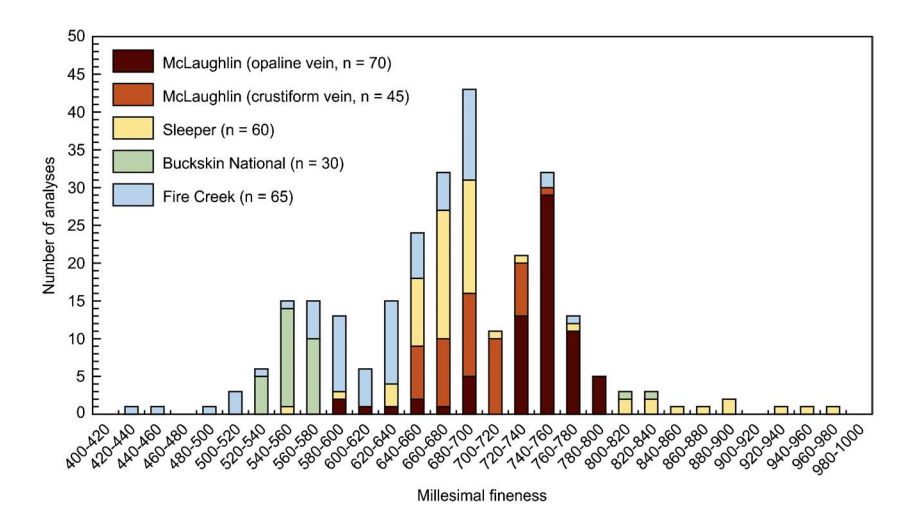
Microanalysis data are provided in Electronic Supplementary Material (ESM) Table 1. Euhedral to subhedral crystals of pyrargyrite, which are up to $\sim\!200~\mu m$ in size, are present throughout the originally microspherical matrix surrounding the gold dendrites (Figs. 3a and 4a–d). The originally

nally microspherical matrix surrounding the crystal is deformed (arrows), which is interpreted to have occurred as a result of crystal growth in the gel-like material. **e** Pyrargyrite encapsulated by euhedral quartz grown through recrystallization of the non-crystalline silica in the matrix. The pyrargyrite forms small complexly shaped grains and dendrites (arrows). The originally microspherical matrix surrounding the euhedral quartz crystals shows concentric banding, interpreted to have formed as a result of maturation of the non-crystalline microspherical silica. **f** Pyrargyrite grains surrounded by quartz grains that formed through recrystallization of the non-crystalline silica in the matrix. The pyrargyrite occurs in the center of the euhedral quartz and along grain boundaries between adjacent quartz crystals. Complexly shaped gold dendrites are present in the originally microspherical matrix. All images were taken in plane polarized light. *Au* gold, *Pyrg* pyrargyrite, *Sp* sphalerite

microspherical matrix surrounding some of the larger stubby pyrargyrite crystals appears deformed (Fig. 4d). In addition to pyrargyrite, minor pyrite crystals ranging up to $\sim 100~\mu m$ are present, some of which contain galena inclusions. In many cases, clear quartz aggregates and crystals formed



Fig. 5 Millesimal fineness of gold contained in the low-sulfidation epithermal vein samples determined by electron microprobe analysis and energy-dispersive X-ray spectroscopy on a scanning electron microscope. Microanalysis data are given in ESM Table 1



through recrystallization of the originally microspherical matrix encapsulate ore mineral dendrites (Fig. 4c) or small complexly shaped aggregates of ore minerals (Figs. 3b and 4e, f).

Gold dendrites also occur within crustiform quartz veins as shown by Sherlock and Lehrman (1995). The dendrites range from several hundred micrometers to several centimeters in size and are hosted by colloform quartz layers that are dark gray in color. The gold dendrites have complex branching morphologies that taper toward the center of the vein, and commonly terminate in dome shapes. Chemical mapping by μ XRF shows that the centimeter-sized dendrites in the samples are chemically and mineralogically zoned, with elevated concentrations of Ag, Cu, Se, and Zn occurring in the top part of the dendrites (Fig. 6). In the samples investigated, the gold dendrites represent the principal host to gold and little fine-grained gold is present in the colloform quartz bands. The gold has a millesimal fineness of 647 to 748, averaging 693 (n=45; Fig. 5; ESM Table 1).

Optical microscopy shows that the centimeter-scale gold dendrites within the crustiform veins have variable morphologies. The dendrites have complex branching shapes. Spiculose deposits or dome-shaped aggregates are common (Fig. 7a, b). Subhedral pyrargyrite crystals occur in the upper portions of the gold dendrites (Fig. 7a), which may account for some of the chemical zoning observed in the µXRF maps. Small euhedral quartz crystals commonly impinge on the gold (Fig. 7c). Under cross-polarized light, the quartz matrix surrounding the gold dendrites exhibits a mosaic texture (Fig. 7d). The equant shape and grain size of the microcrystalline mosaic quartz mimics that of the relict microspheres.

Etching of one of the centimeter-sized gold dendrites hosted by a crustiform vein confirmed that the gold aggregate is of dendritic morphology (Fig. 8a, b). The gold is intergrown with minor pyrargyrite and pyrite (Fig. 8a). Within the more continuous and massive inner portions of

the dendrite, the gold shows casts of small quartz crystals that were dissolved during the HF treatment (Fig. 8c). Some of the gold shows hopper surfaces (Fig. 8d).

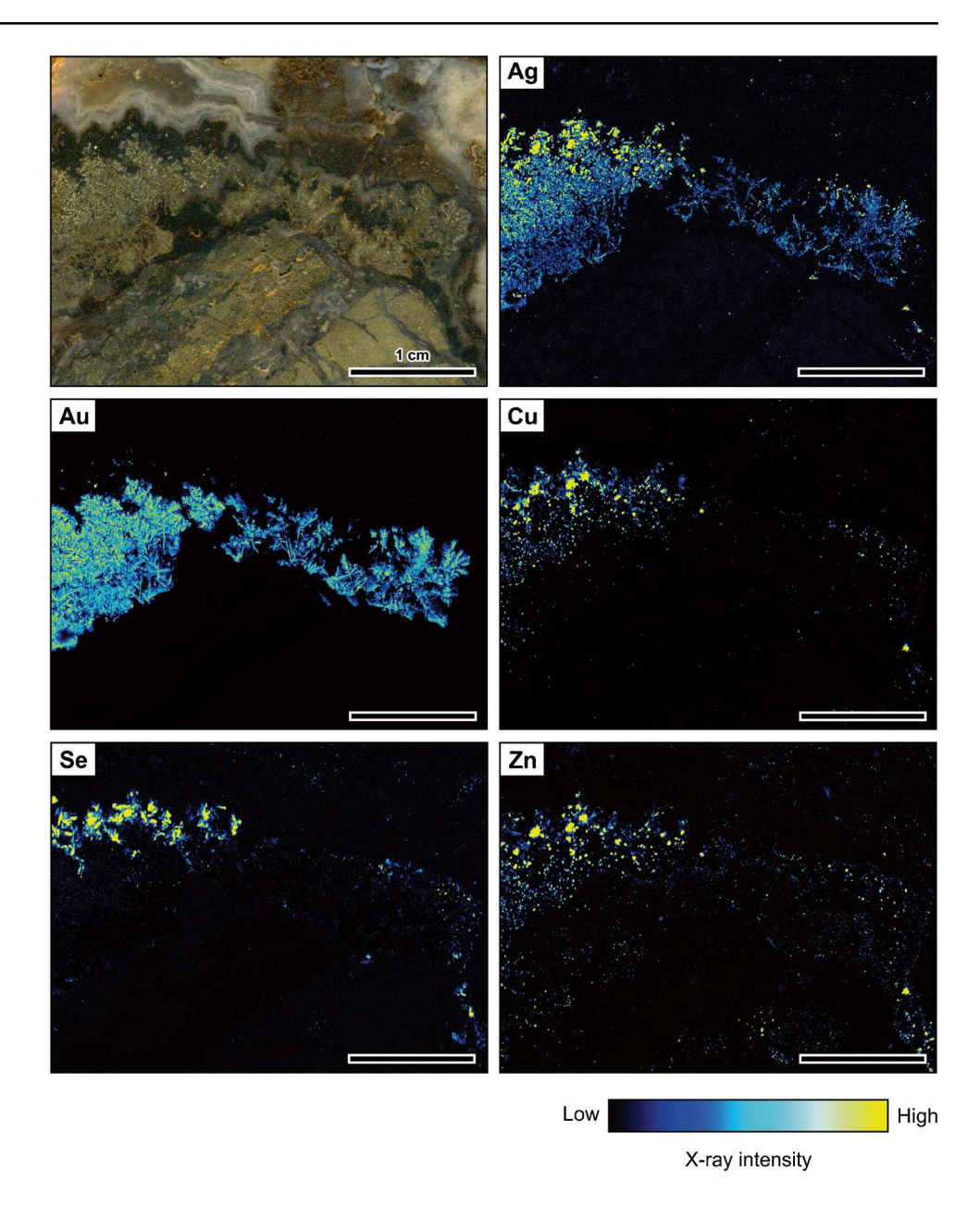
Gold dendrites from Sleeper

Crustiform vein samples from Sleeper contain abundant visible gold. The gold occurs in discrete bands and is hosted by silica that ranges from dark gray to white in color (Fig. 9). Element mapping by µXRF shows that the distribution of Ag is similar to that of Au at the hand specimen scale, although high Ag contents do not always overlap with the highest Au contents. The distributions of Ag and Se are not highly correlative, suggesting that much of the Ag in the samples occurs in gold and not as Ag sulfoselenides (Fig. 9). The samples do not contain detectable amounts of other metals such as Cu and Zn.

The gold distribution varies between individual colloform bands with some containing coarse dome-shaped gold dendrites that are spaced out along the bands (Fig. 10a). Other bands consist of nearly continuous ribbons of gold (Fig. 10b). Relict microspheres ranging from 1 to 5 µm in size are preserved in some colloform bands and are isotropic in cross-polarized light. Individual relict microspheres are outlined by cavities that have sickle-like shapes. However, many bands are composed of microcrystalline quartz (Fig. 10c) that is anisotropic in cross-polarized light (Fig. 10d). The microcrystalline quartz has irregular and interpenetrating grain boundaries and exhibits a mosaic texture (Fig. 10d, f). The size of the quartz grains in the mosaic quartz varies between different colloform bands, ranging from 1 to 75 µm. Zones of mosaic quartz having different grain sizes locally define folds. In some of the bands, doubly terminated quartz crystals appear to have grown within the recrystallized, previously microspherical matrix, forming textures identical to those observed at McLaughlin.



Fig. 6 Sample photograph and corresponding Ag, Au, Cu, Se, and Zn maps of a gold dendrite in a crustiform vein sample from the McLaughlin deposit in California. The element maps show that the dendrite is chemically zoned from bottom to top. The element maps were obtained by μXRF



The colloform bands consisting of variably preserved and recrystallized microspheres alternate with bands that have other textural characteristics. This includes abundant bands composed of microcrystalline adularia and quartz. Adularia in these bands forms euhedral, rhomb-shaped, 5–20 µm large grains that are randomly distributed showing no preferred orientation. The adularia is usually hosted by mosaic quartz. The top surfaces of some of the adularia-bearing bands are wavy and may represent sections through mammillary or ripple-mark-like band surfaces as described by Saunders (1990). Rare bands of comb quartz and colloform bands comprised of chalcedony also occur in the samples. The chalcedony is composed of crystal fibers oriented perpendicular to the colloform bands. The chalcedonic colloform bands consist of alternating

bands of chalcedonic fibers, each having a thickness of up to $\sim 20~\mu m$. Chalcedonic colloform bands can be recrystallized, forming a mosaic texture in cross-polarized light.

In the samples investigated, gold occurs exclusively within the originally microspherical colloform bands and bands of microcrystalline mosaic quartz. Gold dendrites are up to 1.0 mm in size and are dome-shaped or resemble small porous mounds (Fig. 10c, d). These dendrites commonly protrude into adjacent colloform bands. Along the margins, the branches of the gold dendrite are delicate in nature (Fig. 10c-f). Gold in the central portions of the dendrites is more massive in thin section and this coarse gold can be up 75 μ m across. The gold dendrites have a millesimal fineness of 548 to 963, averaging 711 (n = 60; Fig. 5; ESM Table 1).



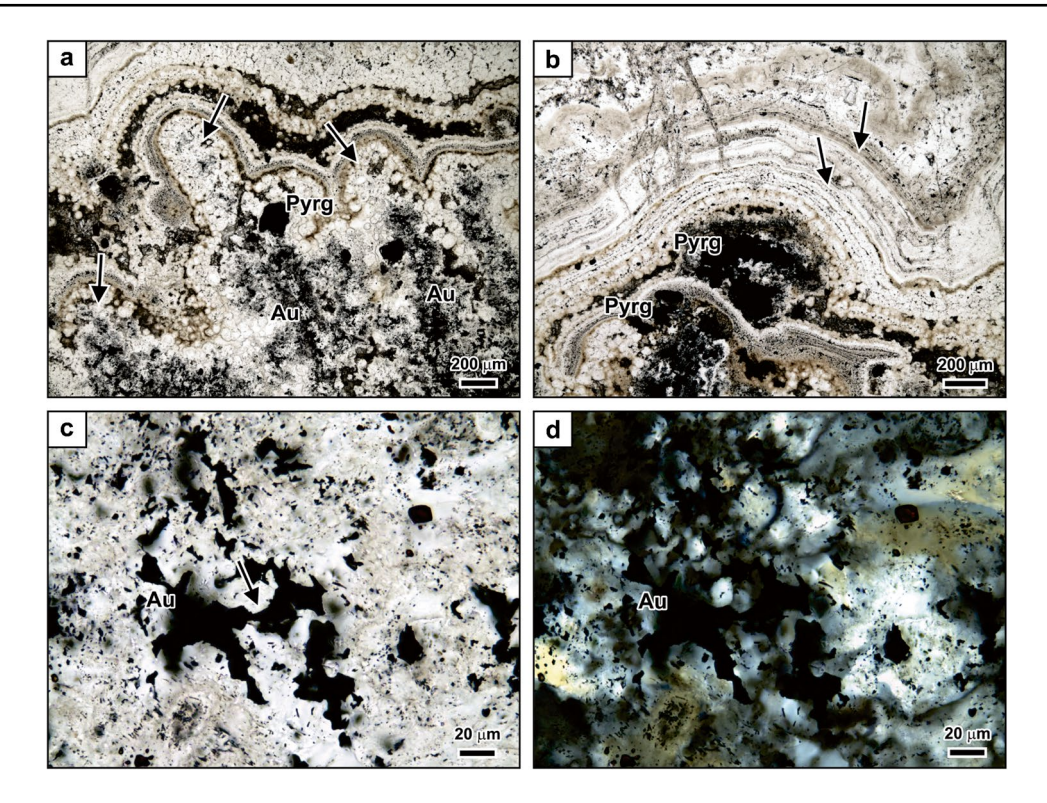


Fig. 7 Photomicrographs of ore mineral textures in crustiform veins from the McLaughlin deposit in California. a Large gold dendrite hosted in mosaic quartz. The silica forms a spiculose deposit (arrows) that hosts individual branches of the dendrite. Some pyrargyrite crystals are present along the tips of the gold dendrite. Plane polarized light. b Dome-shaped ore mineral dendrites hosted by mosaic quartz. Pyrargyrite is the most abundant ore mineral. Unmineralized, banded silica layers (arrows) that have a smooth appearance occur on top

of the mineralized silica layer. Plane polarized light. $\bf c$ High-magnification image of gold forming part of a large dendrite. The gold is surrounded by quartz crystals that formed through recrystallization of the formerly microspherical matrix. Some small quartz crystals impinge on gold along euhedral crystal faces (arrow). Plane polarized light. $\bf d$ Cross-polarized light image of the same field of view showing that the quartz hosting the gold dendrite exhibits a mosaic texture. Au gold, Pyrg pyrargyrite

Similar to McLaughlin, textural relationships between gold and the matrix appear to have been modified as a result of recrystallization of the non-crystalline silica microspheres to quartz. Small (10–50 μm) euhedral quartz crystals are commonly present along the contacts within the gold (Fig. 10c). The small euhedral quartz crystals show irregular extinction patterns resembling those of mosaic quartz. The small quartz crystals lack primary growth zoning and do not contain primary fluid inclusions. The textural relationships suggest that quartz growth occurred as a result of the recrystallization of the originally microspherical matrix. During recrystallization, the original dendritic gold has been deformed and is now in some places encapsulated within the newly formed quartz crystals.

A dome-shaped gold dendrite hosted in microspherical silica was selected for etching with HF. The multi-branching dendrite displays abundant dimples and casts of microspheres or fused microspheres that were dissolved during the HF treatment (Fig. 11a). Casts of quartz crystals dissolved by acid treatment are present (Fig. 11a). The gold surfaces are typically smooth (Fig. 11a–c). At high magnification, a

distinct microtopography consisting of steps and terraces can be observed (Fig. 11c, d).

Naumannite dendrites from Buckskin National

Crustiform vein samples from Buckskin National contain spectacular centimeter-sized naumannite dendrites. The dendrites appear to have grown approximately perpendicular to colloform bands and persist through multiple bands (Fig. 12). They vary in morphology from having narrow bases and wide tops to being more uniform with the tops and bottoms having similar widths. The larger dendrites are spaced laterally along the colloform host bands (Fig. 12). Elemental mapping by µXRF reveals that naumannite is also present in the mineralized bands that occur between the colloform bands hosting the dendrites (Fig. 12). The dendrites exhibit chemical zoning, with Au and Zn occurring in higher concentrations at the base of the dendrites than at the top. In addition to the large naumannite dendrites, some small freibergite dendrites occur that are characterized by an enrichment in Cu in the µXRF maps (Fig. 12).



Fig. 8 Secondary electron images showing the morphology of a gold dendrite from the McLaughlin deposit in California. a Outer portion of a multi-branching gold dendrite. Individual branches are delicate and have dendritic shapes. The gold is intergrown with pyrite. **b** Delicate branches of a gold dendrite. c Massive portion of a gold dendrite showing casts of quartz crystals (arrows) that were dissolved during HF treatment. d Surface of massive gold showing hoppers (arrows). Py pyrite

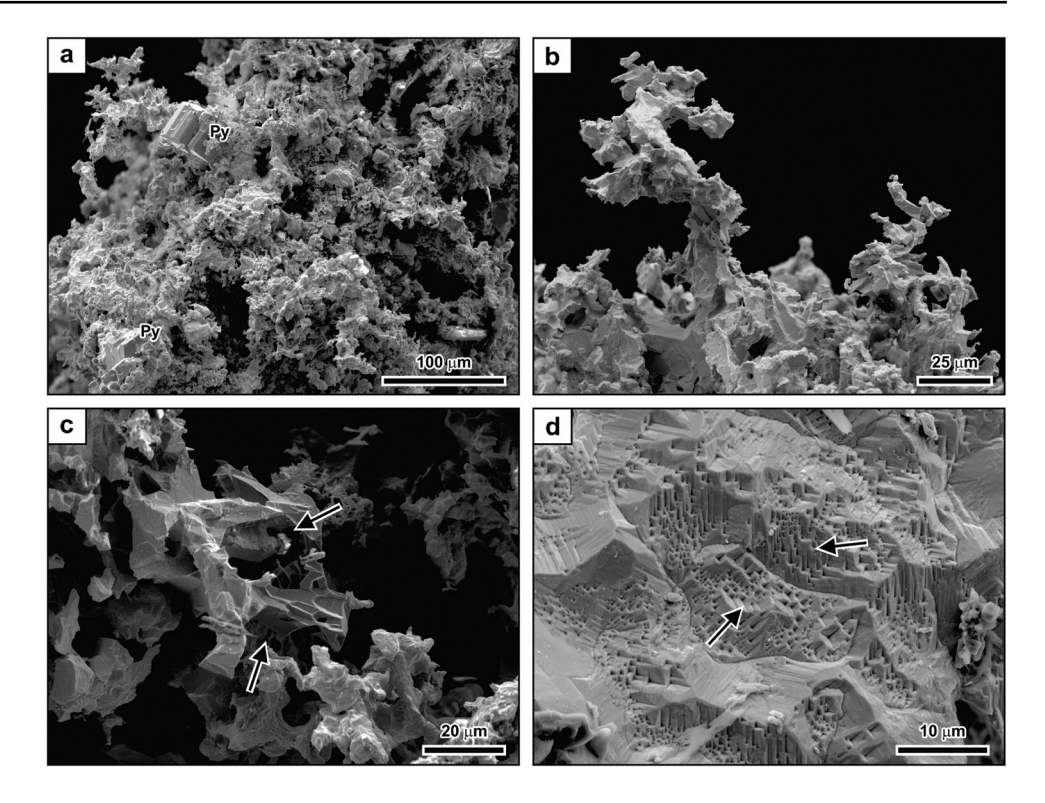
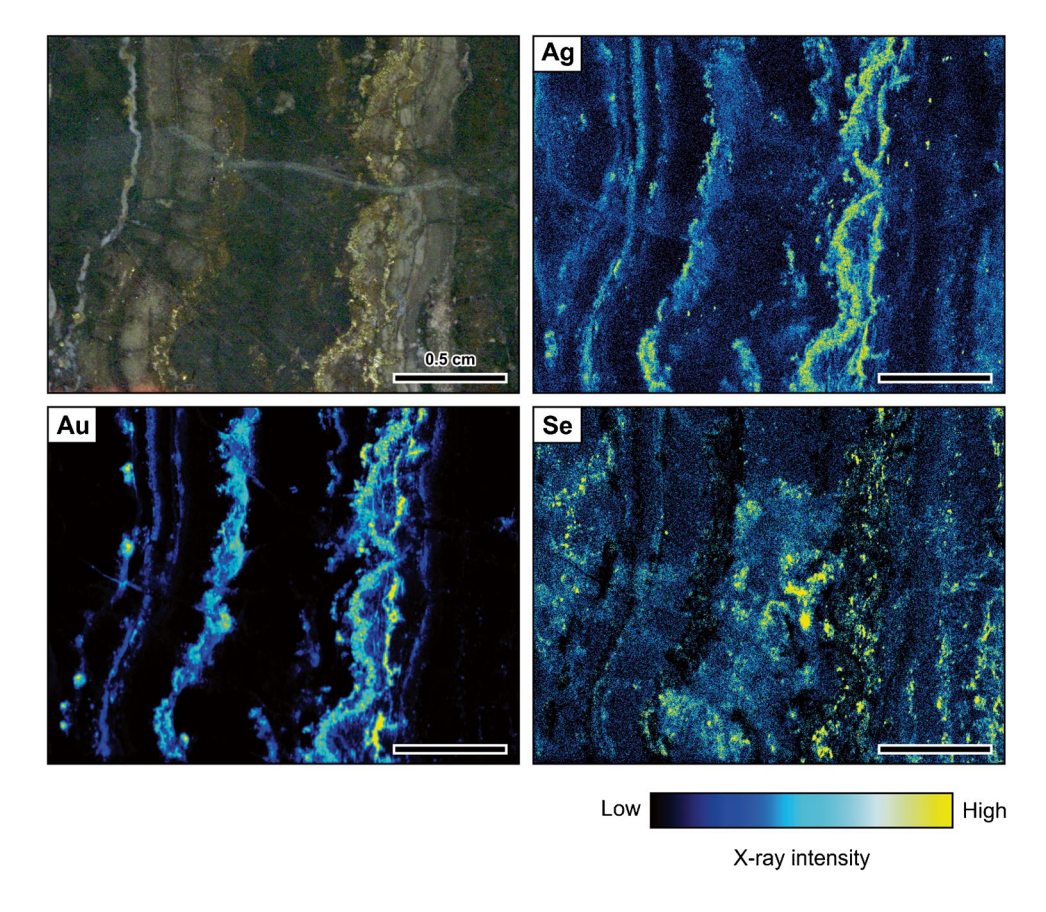


Fig. 9 Sample photograph and corresponding Ag, Au, and Se maps of gold-rich bands in a crustiform vein sample from the Sleeper deposit in Nevada. The element maps show that much of the silver in the vein occurs within the same bands. The element maps were obtained by μXRF





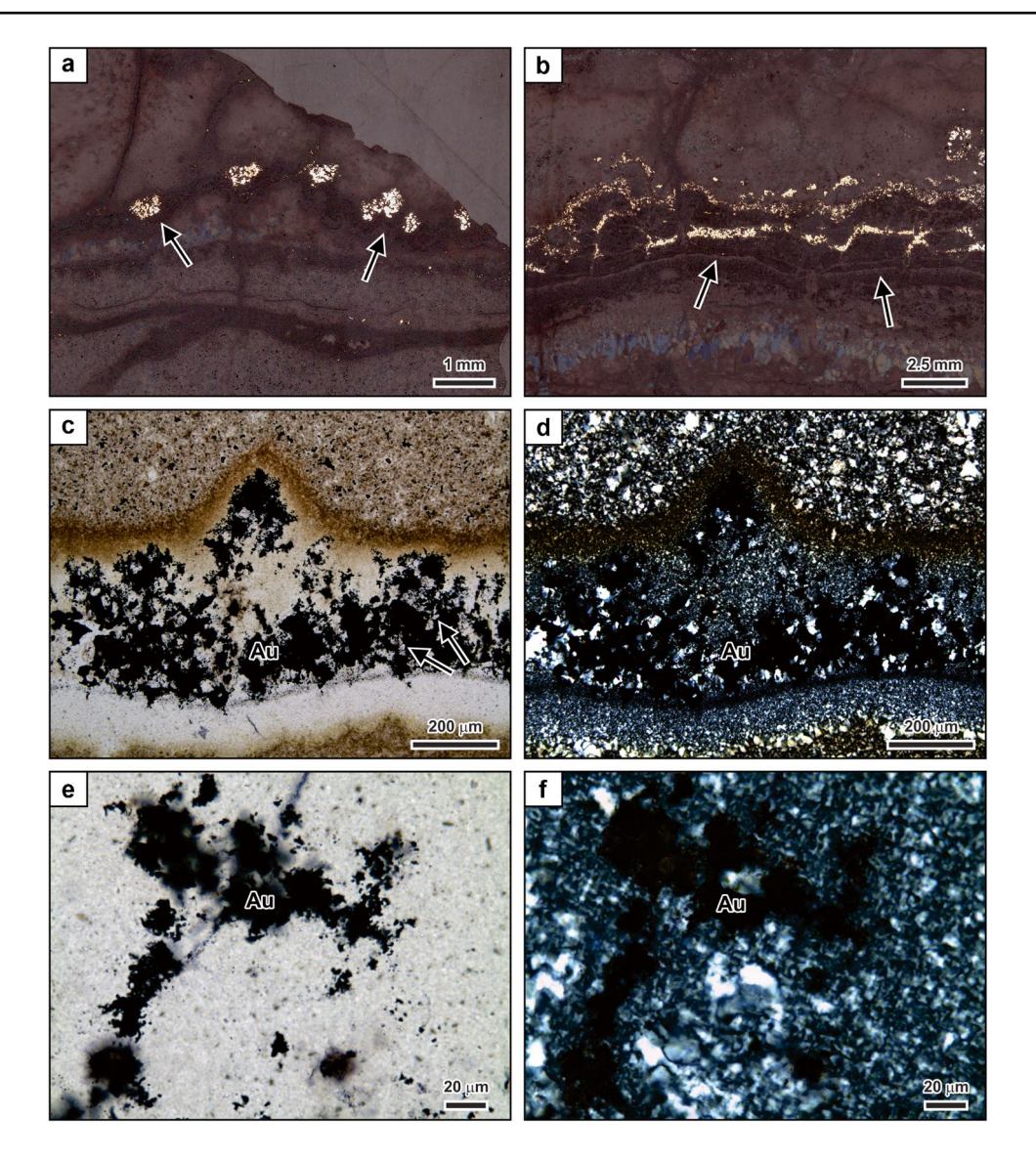


Fig. 10 Photomicrographs of ore mineral textures in crustiform veins from the Sleeper deposit in Nevada. a Colloform bands containing dome-shaped gold dendrites (arrows) that occur in approximately equal spacing along the bands. Reflected light. b Colloform band containing nearly continuous ribbons of gold. The top of the band is wavy (arrows). Reflected light. c Gold dendrites located in a colloform band of quartz. The margins of the dendrites are delicate in shape and intergrown with the matrix. Small euhedral quartz crystals occur within massive gold (arrow). Plane polarized light. d Crosspolarized light photomicrograph of the same field of view showing that the fine-grained quartz matrix of the gold dendrite is character-

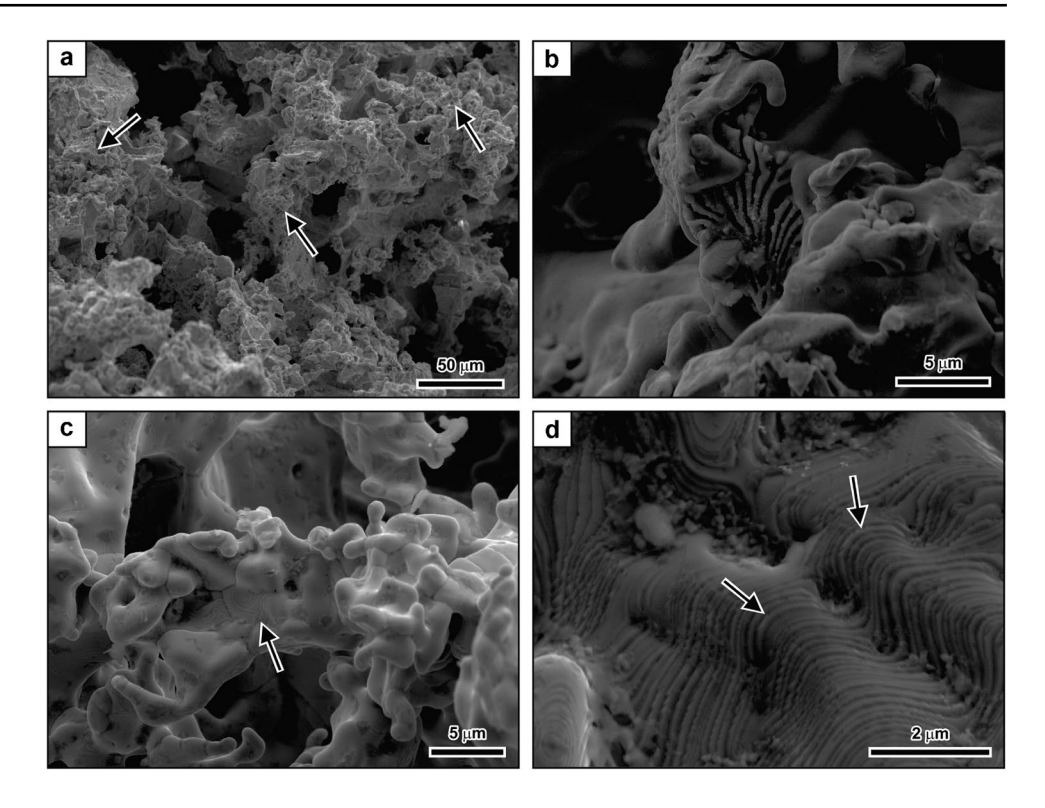
ized by a mosaic texture. **e** High-magnification image showing the contact relationship between gold and the surrounding quartz matrix. The quartz forming the matrix around the gold is microcrystalline and appears to have formed through recrystallization of non-crystalline silica that originally occurred as microspheres. Some gold grains are roughly the same size as the microcrystalline quartz and are distributed in dendritic patterns within the finer-grained matrix. Plane polarized light. **f** Cross-polarized light photomicrograph of the same field of view showing the microcrystalline nature of the quartz matrix. Plane polarized light. Au gold

Optical petrography shows that the large naumannite dendrites are of complex shapes and multi-branching. The wiry naumannite interfingers with the fine-grained quartz matrix, with quartz forming ~50% of the area occupied by the dendrite (Fig. 13a). The colloform bands hosting the dendrite are entirely recrystallized and show a mosaic texture in cross-polarized light (Fig. 13b). The grain size of the anhedral quartz grains forming the mosaic texture is

commonly smaller within the naumannite dendrites than in the surrounding matrix. The size and equant shape of the mosaic quartz resemble the characteristics of the precursor silica microspheres (Fig. 13b). Similar to McLaughlin and Sleeper, recrystallization of the originally microspherical matrix appears to have modified the shape of the naumannite. Dendrite branches consist of naumannite aggregates with small interstitial quartz crystals (Figs. 13c, d). Other



Fig. 11 Secondary electron images showing the morphology of a gold dendrite from the Sleeper deposit in Nevada. a Surface of the gold dendrite displaying abundant dimples and small casts of microspheres or fused microspheres (arrows) dissolved during HF treatment. In addition, some casts of quartz crystals are present. **b** High-magnification image of the surface of the gold showing a dendritic growth structure. c Dendrite branches with a distinct microtopography consisting of steps and terraces (arrow). d High-magnification image of the gold dendrite exhibiting a microtopography of steps and terraces (arrows)



ore minerals present include small dendrites of sphalerite (Fig. 13c) and isolated or composite grains of chalcopyrite, fischesserite (Ag₃AuSe₂), galena, pyrite, and gold.

Electron microprobe analysis showed that the naumannite from Buckskin National contains 72.80 to 75.89 wt% Ag, 21.21 to 24.60 wt% Se, and 1.74 to 2.29 wt% S (n=14; ESM Fig. 1; ESM Table 2). Concentrations of up to 0.15 wt% Cu, 0.22% Hg, and 0.41 wt% Pb were recorded (ESM Table 2). The gold at Buckskin National has a millesimal fineness of 523 to 822, averaging 571 (n=30; Fig. 5; ESM Table 1).

One naumannite dendrite treated with HF shows the complex, multi-branching morphology (Fig. 14a, b) that is consistent with the observations in thin sections. At high magnification, the etched naumannite dendrite shows variable surface characteristics ranging from smooth and rounded to crystalline (Fig. 14 c, d).

Naumannite dendrites from Fire Creek

Crustiform veins at Fire Creek also contain silver-grey naumannite dendrites. The dendrites occur scattered along certain colloform quartz bands or form thick, ribbon-like bands that are almost exclusively composed of naumannite (Fig. 15). Dendrites have grown nearly perpendicular to the colloform bands and are 1–3 mm in size. The colloform quartz bands hosting the dendrites are distinctly white. Chemical mapping by μXRF shows that Au enrichment occurs in a narrow zone immediately below the base of the ribbon-like naumannite as well as in discrete grains toward

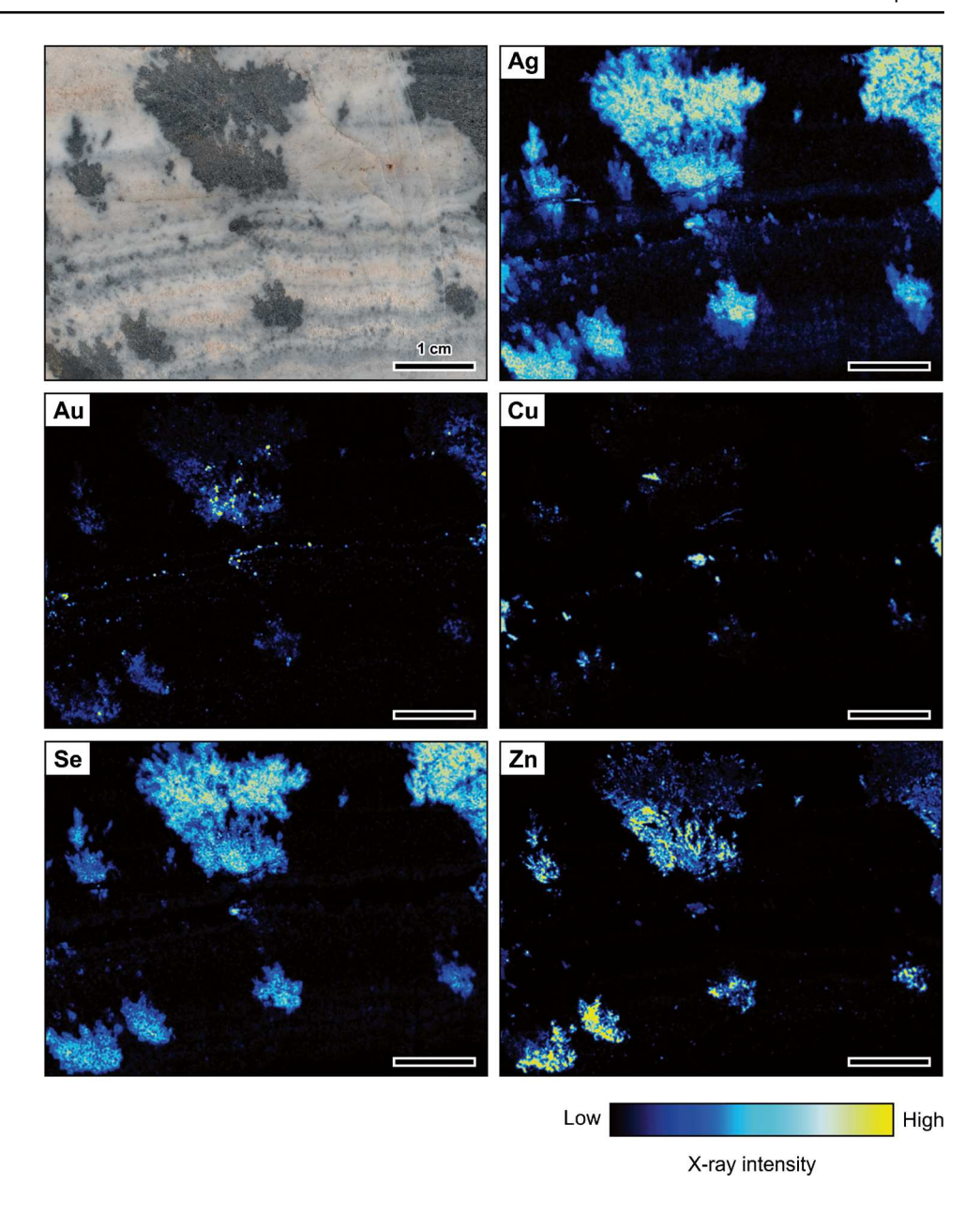
the top of the naumannite dendrites. The distribution of Se mimics the one of Ag. The top of the naumannite zone is characterized by an enrichment in Cu and Zn (Fig. 15).

The naumannite dendrites in thin section are comparably massive and not as delicate as those from the Buckskin National deposit (Fig. 16a). Individual branches can be recognized but are only up to 250 µm wide. More delicate textures can be observed at the base of the naumannite dendrites and the top of individual branches where the naumannite interfingers with the surrounding quartz matrix (Fig. 16a). The quartz matrix is rich in cavities and shows a mosaic texture under cross-polarized light. Similar to Buckskin National, the grain size and shape of the mosaic quartz mimics the characteristics of the precursor silica microspheres at high magnification (Fig. 16b). However, clear euhedral quartz crystals also occur abundantly throughout the recrystallized quartz matrix, with quartz of both morphologies being in contact with the naumannite. Individual euhedral quartz crystals are typically 20-30 µm in size and lack growth zoning defined by fluid inclusions (Fig. 16b). Pyrite, sphalerite, and gold are common and occur as discrete inclusions or larger composite grains with the naumannite. Parts of the naumannite dendrites as well as individual naumannite grains are encapsulated in calcite (Fig. 16c, d).

Electron microprobe analysis showed that the naumannite from Fire Creek contain on average 72.71 to 74.44 wt% Ag, 24.23 to 26.11 wt% Se, and 0.71 to 0.88 wt% S (n = 20; ESM Fig. 1; ESM Table 2). The Te concentration of the naumannite ranges up to 0.30 wt%



Fig. 12 Sample photograph and corresponding Ag, Au, Cu, Se, and Zn maps of naumannite dendrites in a crustiform vein sample from the Buckskin National deposit in Nevada. The elemental maps show that the naumannite dendrites are chemically zoned from bottom to top. The element maps were obtained by μXRF



(ESM Table 2). Compositional analysis showed that gold at Fire Creek has a millesimal fineness of 428 to 779, averaging 624 (n = 65; Fig. 5; ESM Table 1).

A naumannite dendrite etched by HF shows textural characteristics consistent with those observed in thin section. The dendritic grain appears more massive with fewer delicate branches. Many of the smaller branches of the dendrite are crystalline and are composed of small intergrown naumannite grains (Fig. 17a, b). Casts of large euhedral quartz crystals dissolved during HF treatment are present in more massive naumannite (Fig. 17a–d).

Discussion

Colloform bands hosting ore mineral dendrites

In the low-sulfidation epithermal vein samples investigated, ore mineral dendrites are located within specific colloform bands that have unique microtextural characteristics. At McLaughlin and Sleeper, electrum dendrites are located in discrete bands that primarily contain gold, referred to as gankin bands by Tharalson et al. (2019). At



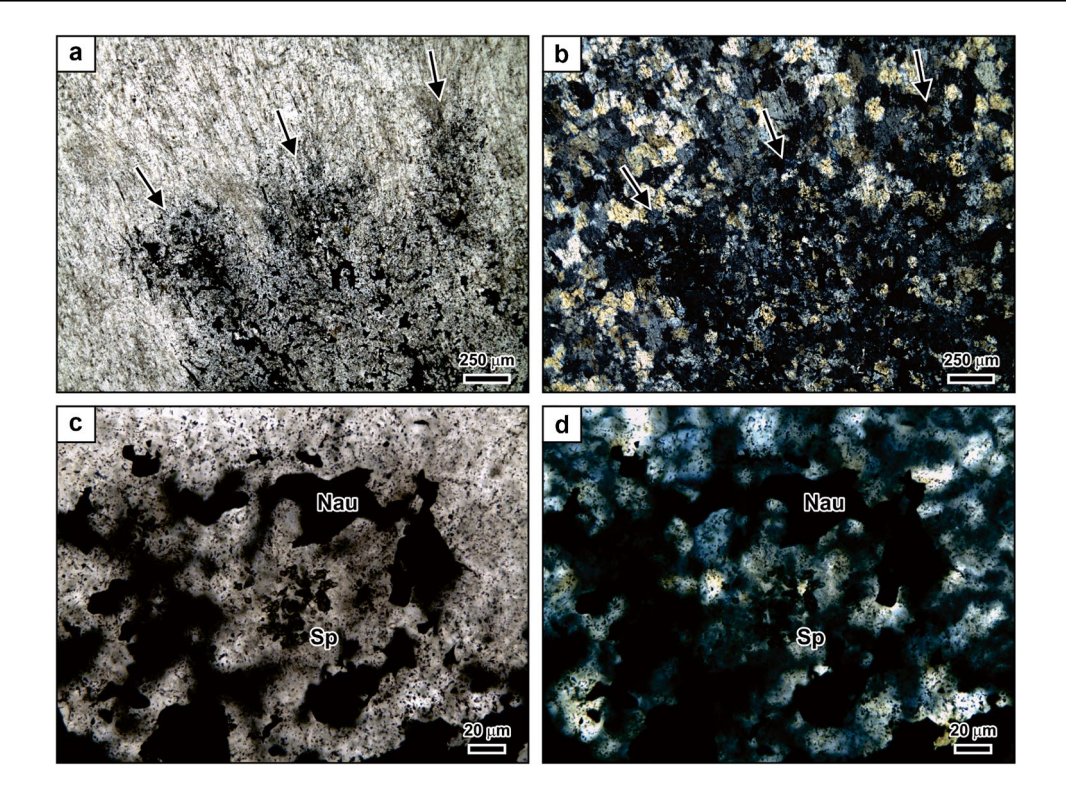


Fig. 13 Photomicrographs of ore mineral textures in crustiform veins from the Buckskin National deposit in Nevada. a Top of a large naumannite dendrite located in quartz that shows a ghost-bladed texture. The backbones of three dendrite branches (arrows) are clearly visible. Plane polarized light. b Corresponding cross-polarized light image showing that the ghost-bladed quartz exhibits a mosaic texture. The grain size of the quartz is variable and generally smaller within and

around the naumannite dendrite than in the surrounding matrix. **c** High-magnification image showing the contact relationship between the naumannite and the surrounding quartz matrix. The microcrystal-line quartz in the colloform band presumably formed through recrystallization of non-crystalline silica originally occurring as microspheres. **d** Corresponding cross-polarized light image showing the mosaic texture of the quartz. *Nau* naumannite, *Sp* sphalerite

Fig. 14 Secondary electron images showing the morphology of a naumannite dendrite from the Buckskin National deposit in Nevada. a Low-magnification image showing the dendritic nature of the naumannite. b Dendritic naumannite consisting of delicate branches. c Dendrite branch containing small naumannite crystals (arrows). d High-magnification image showing that some branches consist mostly of small naumannite crystals (arrows)

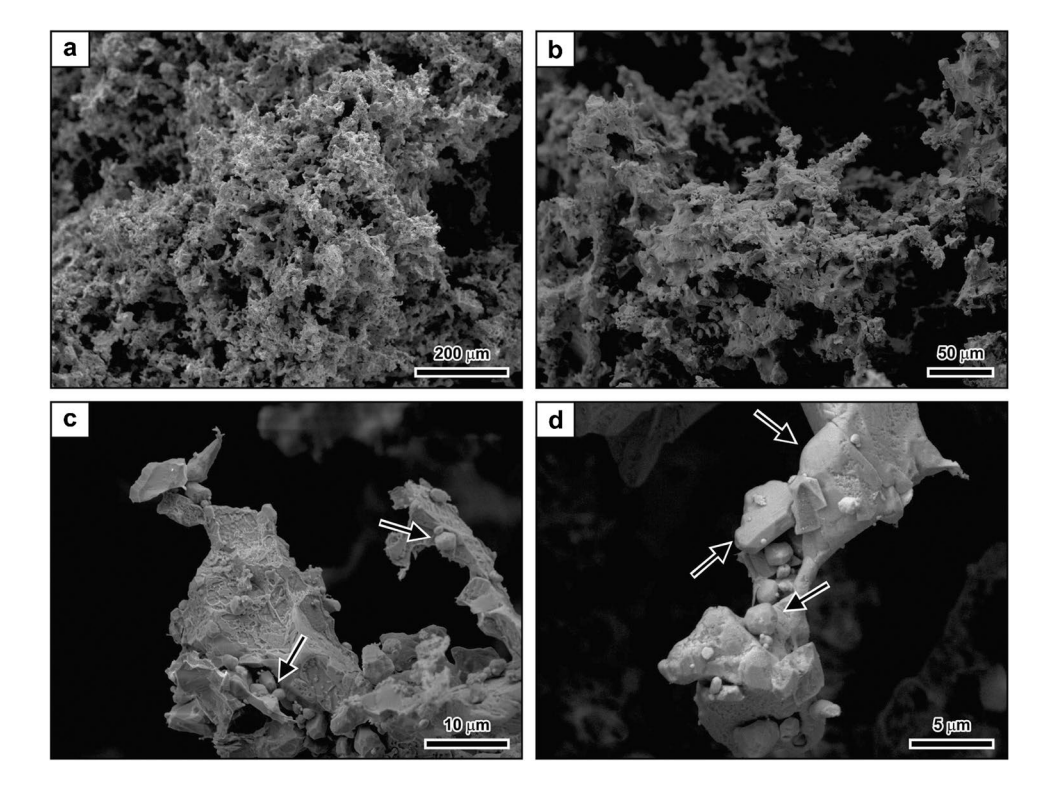
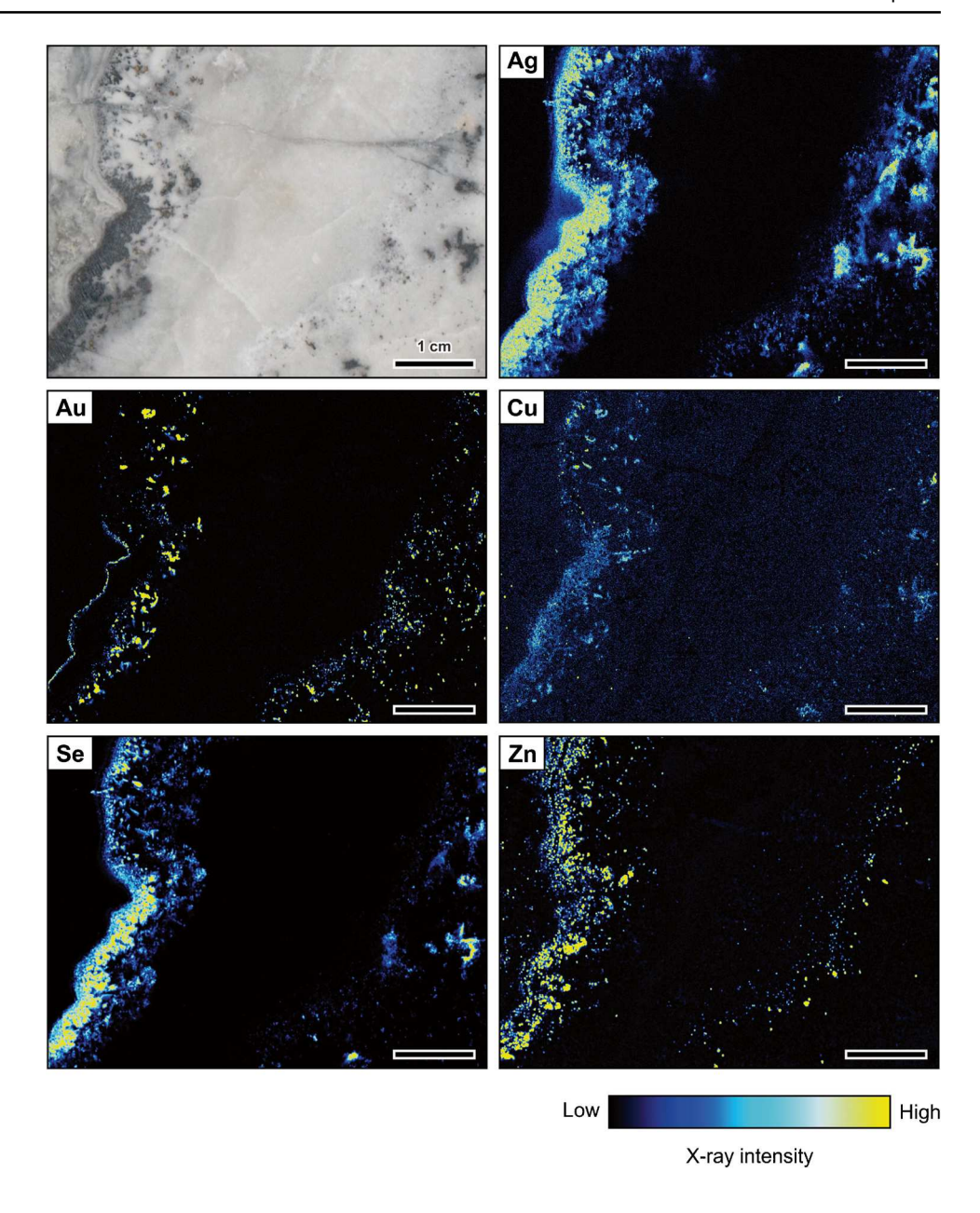




Fig. 15 Sample photograph and corresponding Ag, Au, Cu, Se, and Zn maps of mineralized bands in a crustiform vein sample from the Fire Creek deposit in Nevada. The element maps show that the band of dendritic naumannite is chemically zoned. The element maps were obtained by μXRF



Buckskin National and Fire Creek, naumannite dendrites are located in distinct light gray metallic bands, referred to as ginguro bands by previous workers (Takeuchi and Shikazono 1984; Shimizu et al. 1998; Leavitt et al. 2004; Saunders et al. 2008; Shimizu 2014). The mineralized bands are composed of relict microspherical silica or mosaic quartz that formed from a non-crystalline precursor through a process of maturation and recrystallization.

Preserved 1–5 µm relict silica microspheres are common in the mineralized colloform bands in the samples from McLaughlin and Sleeper. In rare areas, they are still noncrystalline as they are isotropic in cross-polarized light. Non-crystalline silica microspheres form sinters around hot springs (Jones et al. 1997; Herdianita et al. 2000; Campbell et al. 2002; Guidry and Chafetz 2003; Lynne and Campbell

2004; Rodgers et al. 2004; Fernandez-Turiel et al. 2005) and scalings in geothermal power plants (Rothbaum et al. 1979; Brown 2011; Meier et al. 2014; Zarrouk et al. 2014; Taksavasu et al. 2018; van den Heuvel et al. 2018). This microspherical form of non-crystalline silica is classified as opal-A_G (Smith 1998).

Studies on silica sinters (Campbell et al. 2001, 2002; Lynne and Campbell 2004; Rodgers et al. 2004; Lynne et al. 2005, 2007; Jones 2021) and geothermal scales (Reyes et al. 2002; Raymond et al. 2005) have shown that opal- A_G is thermodynamically unstable and matures and recrystallizes over time. The maturation and recrystallization process involves the transformation of non-crystalline opal- A_G into opal-CT, which in turn recrystallizes into opal-C and then into quartz. Relict microspheres can be petrographically



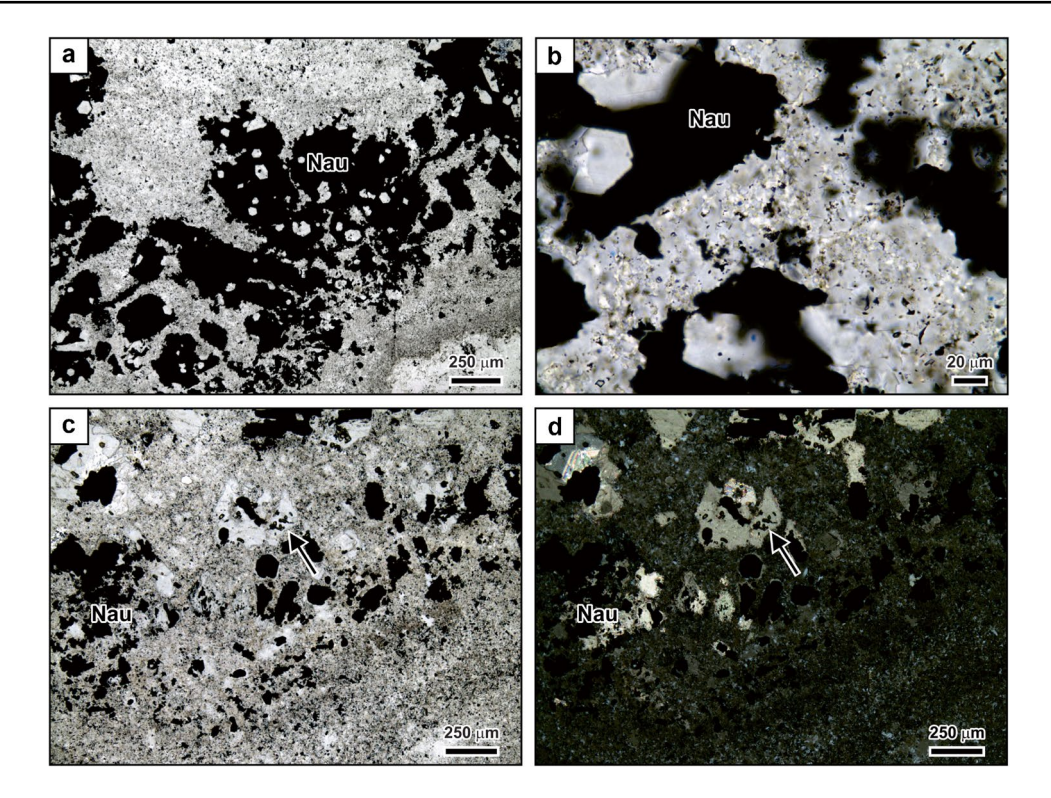
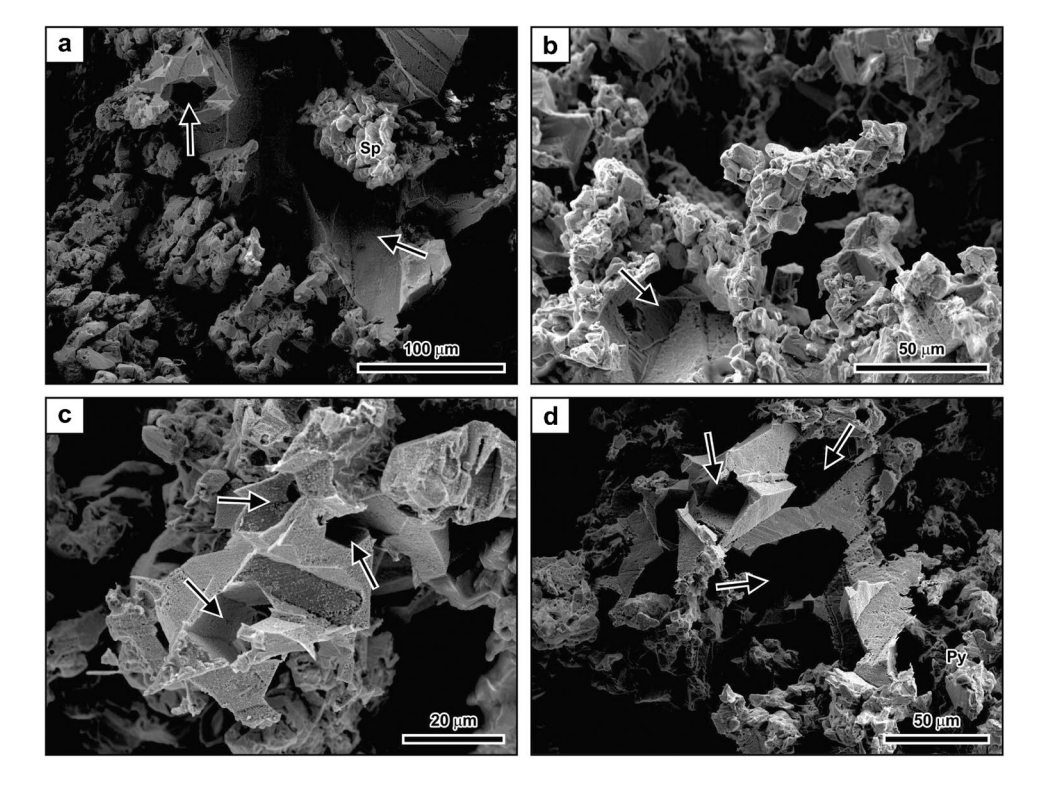


Fig. 16 Photomicrographs of ore mineral textures in crustiform veins from the Fire Creek deposit in Nevada. a Naumannite dendrites located within a colloform quartz band. Plane polarized light. b High-magnification photomicrograph illustrating the contact relationships between the naumannite and the surrounding quartz matrix. Small euhedral quartz crystals occur. The microcrystalline quartz in the colloform band presumably formed through recrystallization of

non-crystalline silica originally occurring as microspheres. Slightly cross-polarized light. **c** Colloform quartz band containing dendritic naumannite aggregates. Some of the naumannite grains are encapsulated by calcite (arrow). Plane polarized light. **d** Corresponding crosspolarized light photomicrograph showing that the colloform quartz band exhibits a fine mosaic texture. Calcite forms a halo around some of the naumannite grains (arrow). *Nau* naumannite

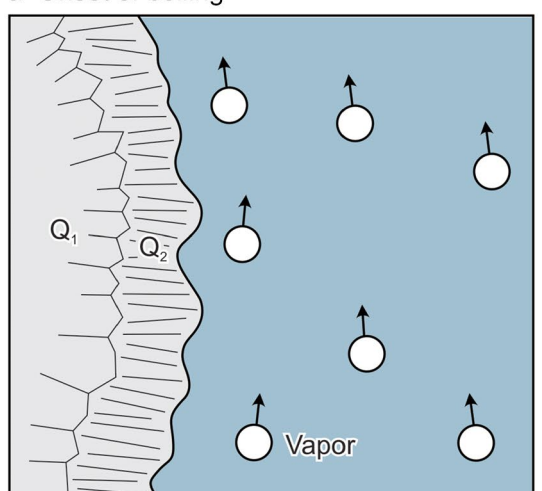
Fig. 17 Secondary electron images showing the morphology of a naumannite dendrite from the Fire Creek deposit in Nevada. a Naumannite dendrite intergrown with sphalerite. More massive naumannite shows casts of quartz crystals (arrows) dissolved during HF treatment. b Delicate branch of the naumannite dendrite that consists of intergrown crystals, some of which show well-developed crystal faces. c Massive naumannite aggregate that shows casts of quartz crystals (arrows) dissolved during HF treatment. d Casts of quartz crystals (arrows) dissolved during the HF treatment within a massive naumannite aggregate. The naumannite is intergrown with minor pyrite. Py pyrite, Sp sphalerite



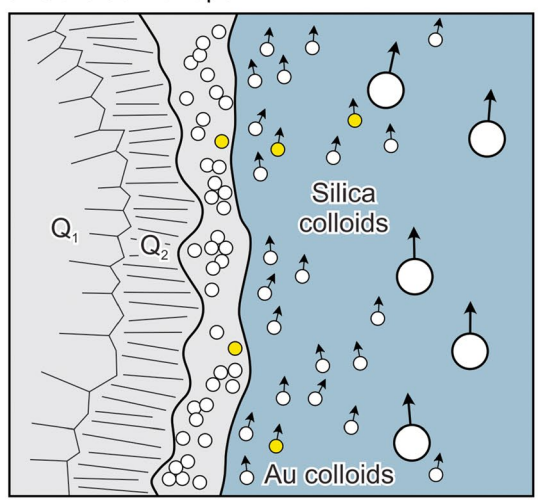


Model of dendrite growth along vein walls involving colloidal gold and silica transport (Saunders 1990)

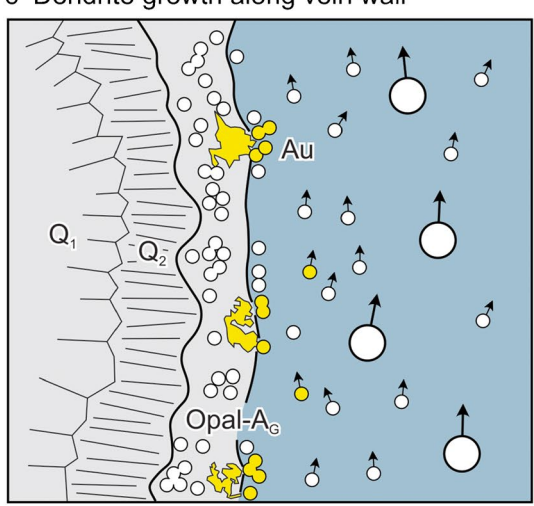
a Onset of boiling



b Colloidal transport

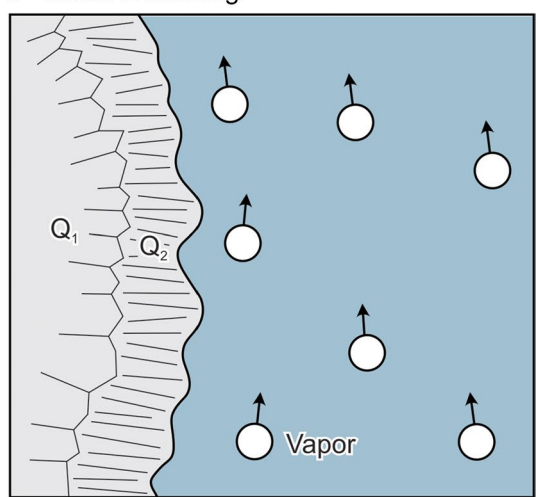


c Dendrite growth along vein wall

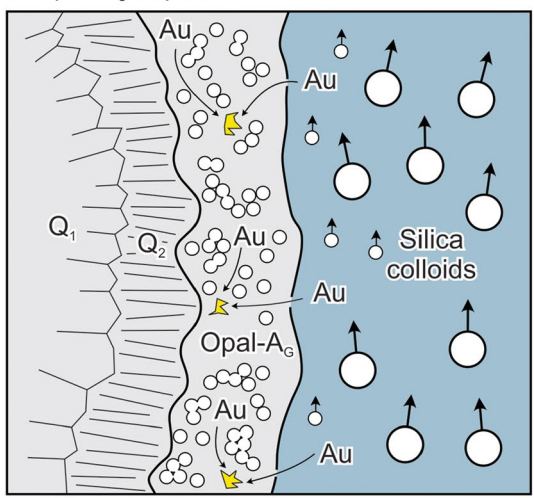


Model of dendrite growth within previously deposited silica matrix (Monecke et al. 2022)

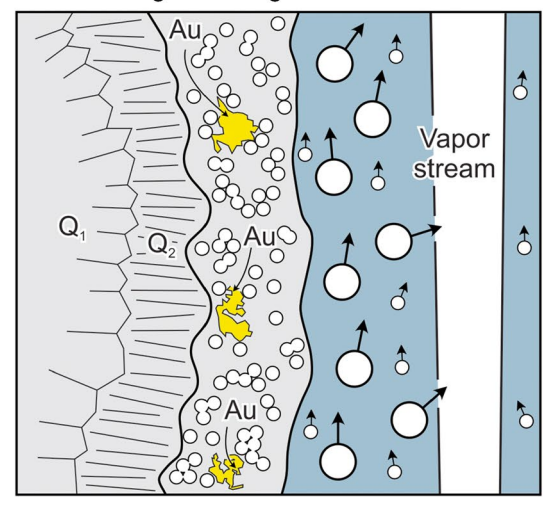
a Onset of flashing



b Opal-A_G deposition



c Dendrite growth in gel matrix





◄Fig. 18 Endmember models for electrum dendrite growth in low-sulfidation epithermal deposits. Saunders (1990) proposed that electrum dendrites grow from colloids transported by the hydrothermal liquids. The model assumes that the gold dendrites grow contemporaneously with the deposition of the silica host along the vein walls. The model by Monecke et al. (2023) suggests that electrum dendrites grow within a previously formed silica matrix below the surface of the microspherical host. Gold could be transported in solution

identified in many of the mineralized bands at McLaughlin and Sleeper. However, their original presence can only be inferred in the crustiform vein samples from Buckskin National and Fire Creek based on the grain size and equant shape of the mosaic quartz. The silica microspheres likely originally present have recrystallized to mosaic quartz having interpenetrating grain boundaries as described by Lovering (1972) and Dong et al. (1995).

It is proposed here that the colloform mineralized bands in the low-sulfidation epithermal vein samples formed by accumulation of microspheres of opal-A_G, as previously suggested by Sherlock and Lehrman (1995), Taksavasu et al. (2018), and Zeeck et al. (2021). The silica deposits could have varied in nature. Some of the microspherical material may have formed spiculose or dendritic deposits resembling spiculose silica sinters (Schinteie et al. 2007) or scales in geothermal wells (Hawkins et al. 2014; Mroczek et al. 2017; van den Heuvel et al. 2018; Chambefort and Stefánsson 2020). The microspheres may also have formed gel-like masses that were highly permeable due to the amount of water present between the silica microspheres. Deformation textures such as rippled surfaces caused by hydraulic shaping, or gravity-induced sagging, have been previously described from low-sulfidation epithermal deposits (Saunders 1990, 1994; Saunders et al. 2008, 2011; Unger 2008; Aseto 2012; Shimizu 2014). As proposed by Saunders (1990), these textures suggest that the colloform bands originally consisting of opal-A_G may have been gel-like and yielding at the time of deposition, perhaps similar to gel-like silica covering wall-rock clasts blown to surface during the 1989 hydrothermal eruption of Porkchop Geyser in Yellowstone (Fournier et al. 1991; Keith 1992).

Formation of ore mineral dendrites

The textural observations suggest that ore mineral dendrite growth is closely linked to the formation and deposition of microspherical silica. Chemical mapping using μXRF combined with high-resolution optical microscopy demonstrated that the ore minerals are only present in specific bands and only occur in bands that contain silica microspheres or their recrystallized equivalents. Ore-bearing colloform bands alternate with colloform bands that are barren and commonly show a chalcedonic microtexture, as previously noted by Zeeck et al. (2021). Two different models have been

previously proposed explaining how ore mineral dendrites form in mineralized colloform silica bands in low-sulfidation epithermal deposits (Saunders 1990; Monecke et al. 2023). Both models differ with respect to the timing relationships between the ore minerals and the surrounding silica host.

Saunders (1990) originally proposed that electrum dendrites contained in low-sulfidation epithermal veins at Sleeper grew from colloids transported by the hydrothermal liquids. He envisaged that colloids were formed in the deeper parts of the hydrothermal system, perhaps as a result of boiling. The colloids were then mechanically transported by the hydrothermal liquid and grew through physical aggregation during upflow of the hydrothermal liquids from the deep reservoir (Saunders 1990; Saunders and Schoenly 1995b). The gold particles would have been deposited through density accumulation where fluid velocity decreased in wider parts of open fractures, or through scavenging of gold from the liquid by charged surfaces at the interface between gold deposited on the wall of the vein and the hydrothermal liquid (Saunders 1990). The model proposed by Saunders (1990) assumes that gold dendrites grew contemporaneously with the deposition of the silica host (Fig. 18), with the silica microspheres providing the structural support for the growing dendrites. Saunders et al. (2011) suggested that colloidal transport is not restricted to gold and that naumannite dendrites in low-sulfidation epithermal veins may have formed by similar processes.

Primary textural relationships observed in the opaline vein samples from McLaughlin support an alternative hypothesis whereby ore mineral growth occurred entirely within the bands of opal- A_G microspheres and not at the interface between the microspherical opal- A_G host and the hydrothermal liquid in the vein (Monecke et al. 2023). In this case, dendrite growth within the silica host would have occurred by diffusion or advection of metals from the liquid flowing through the vein above the surface of the layer of microspheres. Monecke et al. (2023) suggested that the host silica bands would have been permeable enough to allow chemical exchange between the interstitial liquid within the microspherical opal- A_G and the hydrothermal liquid within the central vein opening.

Saunders and Schoenly (1995a) studied the fractal dimensions of electrum dendrites from the National and Sleeper deposits in Nevada. They showed that the morphology and fractal nature of these dendrites could be best explained by a rapid diffusion-limited process. The textural observations of this study are consistent with a model of dendrite growth whereby crystal growth is diffusion-limited as the dendrite shapes resemble Brownian trees (Witten and Sander 1981). Given the low concentrations of metals in hydrothermal liquids (Simmons and Brown 2007), growth of the dendrites requires replenishment of the liquid at the site of mineral formation over the duration of crystal growth. In the case



of the samples from Sleeper, it is striking that the electrum dendrites form small, periodically spaced domes or mounds within the microspherical host. Similarly, the large naumannite dendrites studied from the Buckskin National deposit are relatively equally spaced along the vein and several large dendrites are stacked on top of each other. A diffusion-limited process growth mechanism could explain the spacing between the dendrites that ultimately grew large enough to be macroscopically visible.

Monecke et al. (2023) proposed that the ore mineral dendrites in the opaline vein samples at McLaughlin formed within gel-like bands of opal-A_G, with the microspherical silica providing a framework for the delicate growth of the ore minerals (Fig. 18). This is analogous to crystal synthesis in silica gels. Experimental studies have long made use of silica gel as a medium for the growth of crystals at laboratory conditions (Holmes 1917; Fisher and Simons 1926). In these experiments, a feed solution is poured over a layer of silica gel. Downward diffusion of nutrients from the overhead feed solution causes the growth of the crystals in the chemically inert gel matrix which provides a three-dimensional structure in which the crystals grow and are held in position of their formation. Within days, crystals can be synthesized that range from millimeters to centimeters in size. A wide range of materials have been grown this way, including cadmium oxalate hydrate (Raj et al. 2008), calcium carbonate (McCauley and Roy 1974), copper (Holmes 1917), gold (Holmes 1917; Muzikář et al. 2006), lanthanum tartrate (Kotru et al. 1986), lead iodide (Holmes 1917; Fisher and Simons 1926), lead sulfide (Brenner et al. 1966), mercury iodide (Holmes 1917), silver dichromate (Holmes 1917), silver iodite (Halberstadt 1967), and silver sulfate (Holmes 1917). The growth experiments yield single crystals or polycrystalline aggregates closely resembling those observed in the vein material investigated in this study, ranging from skeletal to dendritic.

The crystal growth experiments show that the control on nucleation of crystals in the gel is of great importance because the growing crystals compete with one another for reactants and competition reduces the size and perfection of the synthesized crystals (Brenner et al. 1966; Raj et al. 2008). The relative amount of nucleation sites can be controlled by adding the overhead solution after variable times of silica gel maturation. In general, the nucleation rate decreases as the age of the gel is increased prior to placing the overhead solution on top of the gel (Raj et al. 2008). This is related to a reduction of the pore size of the gel during maturation, which reduces diffusion of the upper reactants through the gel. The density of the gel has a substantial influence on the morphology of the crystals grown, with skeletal and dendritic morphologies tending to form at increased gel density. This indicates that diffusion-limited crystal growth dominates in the gel media. Diffusion is relatively predominant for the transformation process of the solutes as the viscous nature of the silica gel suppresses convection (Oaki and Imai 2003).

The experimental studies establish that ore mineral dendrites growth within silica gels accumulated along vein walls is a viable process occurring in low-sulfidation epithermal deposits, particularly for thick accumulations of microspheres containing small ore mineral dendrites. However, growth of ore mineral dendrites contemporaneously with the accumulation of silica microspheres might be likely where only limited amounts of silica are deposited from the hydrothermal fluids, as originally envisaged by Saunders (1990). The large ore mineral dendrites in the crustiform vein samples from the four low-sulfidation epithermal deposits studied here may have formed as the microspherical opal- $A_{\rm G}$ host was accumulating as they do not occur in the thick layers of microspherical silica and may not have formed entirely below the surface of the microspherical host.

Textural changes resulting from maturation and recrystallization

Petrographic investigations suggest that three main types of quartz vein textures can be encountered in low-sulfidation epithermal deposits (Bobis 1994; Dong et al. 1995; Etoh et al. 2002; Moncada et al. 2012). This includes primary textures formed through growth of quartz crystals into open space or direct precipitation of silica from the hydrothermal liquids, replacement textures originating from partial or complete replacement of earlier formed gangue minerals such as calcite and adularia by quartz, and maturation and recrystallization textures resulting from the transition of a metastable silica precursor to thermodynamically stable quartz.

The vein samples from the four low-sulfidation epithermal deposits exhibit a wide range of maturation and recrystallization textures. In samples from McLaughlin, Monecke et al. (2023) showed how doubly terminated quartz crystals have grown within the opal-A_G matrix as a result of the transformation of non-crystalline opal-A_G to quartz, which commenced with the development of the concentrically banded silica spheres. When these small euhedral crystals occur in abundance, they competed for space forming aggregates of quartz typified by interpenetrating grain boundaries, yielding the mosaic texture described by Lovering (1972) and Dong et al. (1995). This texture characterized by anhedral to euhedral quartz grains having irregular and interpenetrating grain boundaries appears to be the most common result of the maturation and recrystallization of the non-crystalline silica precursor, as it is recognized in all four deposits studied. In samples where all opal-A_G is matured and recrystallized to quartz, grain size variations in the mosaic quartz define former colloform banding.



With the development of the mosaic texture through maturation and recrystallization, the original textural relationships between the ore minerals and the silica host are modified. In recrystallized colloform bands characterized by the presence of mosaic quartz, the ore minerals commonly are located in vugs that are lined by the fine-grained euhedral quartz crystals. These euhedral quartz crystals have formed after the ore minerals during maturation and recrystallization of the opal- $A_{\rm G}$ matrix (Zeeck et al. 2021; Monecke et al. 2023). The etched ore mineral dendrites from the four deposits studied exhibit abundant casts of these euhedral quartz crystals.

The maturation and recrystallization of the non-crystalline silica host also appears to have resulted in changes to the appearance and distribution of the ore minerals. In some areas, ore mineral grains are randomly distributed throughout the formerly microspherical silica matrix. In other areas where mosaic quartz is present, ore mineral grains occur preferentially along the interpenetrating grain boundaries of the mosaic quartz or are encapsulated within the quartz. This suggests that maturation and recrystallization of the matrix could have been accompanied by small-scale redistribution of the ore minerals. A progression in the textural appearance of gold was observed in the sample from Sleeper. While some of the delicate gold dendrites are present in formerly microspherical silica bands, coarser gold aggregates and patches are present in bands where abundant small euhedral quartz crystals are present along the contacts between the silica host and the gold. The maturation and recrystallization of the matrix appear to have resulted in grain coarsening and morphological changes of the gold.

At Sleeper, the degree of maturation and recrystallization of the non-crystalline silica precursor often varies between adjacent colloform bands. While some of the bands contain preserved relict silica microspheres that are still isotropic, adjacent bands are entirely composed of mosaic quartz. These variations on the sample scale may suggest that the maturation and recrystallization of opal-A_G originally contained in the colloform bands commenced at hydrothermal conditions immediately following silica deposition. Depending on kinetic factors, different microspherical bands may have matured and recrystallized to different degrees, which may also account for the variations in grain size in the mosaic quartz. Laboratory investigations demonstrate that the maturation of non-crystalline silica to quartz can take place within as little as days to months under hydrothermal conditions (Ernst and Calvert 1969; Bettermann and Liebau 1975; Oehler 1976).

Flashing of hydrothermal liquids

The presence of abundant colloform bands of relict silica microspheres or of mosaic quartz formed through maturation and recrystallization in the vein samples from the four low-sulfidation epithermal deposits studied suggests that the hydrothermal liquids forming these veins periodically reached saturation with respect to opal-A. In the epithermal environment, saturation of opal-A in hydrothermal liquids can be achieved due to vapor loss associated with vigorous boiling of the hydrothermal liquids, which is referred to as flashing (Saunders 1990, 1994; Moncada et al. 2012; Saunders and Burke 2017; Taksavasu et al. 2018; Zeeck et al. 2021).

The textural evidence observed here suggests that the ore mineral dendrites grew during deposition of the opal- A_G matrix or immediately after the deposition of the noncrystalline silica microspheres along the vein walls while the opal- A_G was still highly permeable. Ore mineral formation appears to be directly linked to the occurrence of the short-lived flashing events. Vapor loss from the hydrothermal liquid during flashing would represent an effective metal deposition mechanism as dissolved H_2S is lost into the vapor phase causing supersaturation of dissolved metals in the hydrothermal liquid (Weissberg 1969; Brown 1986; Krupp and Seward 1987; Christenson and Hayba 1995; Simmons and Browne 2000).

Thermodynamic modeling by Christenson and Hayba (1995) suggested that the degree of vaporization is a key control on ore mineral formation. Modeling of isothermal vapor loss from a hydrothermal liquid at 230 °C showed that sphalerite and pyrite precipitation commences with the onset of vaporization of the hydrothermal liquid. Sphalerite is stable throughout the process of vaporization whereas pyrite is replaced by chalcopyrite at ~3 wt% vapor loss. Galena saturates at ~3 wt% vapor loss and continues to precipitate throughout the process of vapor generation. Gold precipitation starts at ~6 wt% vapor loss and continues to ~90 wt% vapor loss, with peak precipitation occurring at ~10 wt% vapor loss.

The Christenson and Hayba (1995) thermodynamic model conceptually explains why different colloform silica bands in the samples contain different ore minerals and why ore mineral dendrites are mineralogically zoned from bottom to top. The degree of vapor loss from the liquid may have been different for ore minerals forming at different times in successive silica bands, potentially explaining why the mineralized bands vary in metal associations within individual hand specimens. Similarly, the degree of vapor loss may have changed over time as dendrites were growing in individual bands, explaining the observation that the dendrites changed in composition during growth.

Exploration implications

One of the key implications of this study is that the formation of bonanza-type ore zones in low-sulfidation epithermal



deposits can be linked to the occurrence of fluid flashing. Fluid flashing represents the most likely explanation for the formation of the microspherical silica hosting the ore minerals and likely also caused ore mineral formation (Christenson and Hayba 1995). Short-lived fluid flashing events are common in geothermal systems, being typically triggered by seismic activity (Rowland and Simmons 2012). At surface, these events are manifested by hydrothermal eruptions and the formation of craters that range from tens to hundreds of meters in diameter and are surrounded by low-relief walls formed by excavation of host rocks during the eruption (Muffler et al. 1971; Nairn and Wiradiradja 1980; Hedenquist and Henley 1985; Marini et al. 1993).

This study also casts doubt on previous models assuming that mineralization has to occur at a particular depth below the paleosurface. Mineral precipitation will occur in the deeper subsurface in the region of two-phase liquid and vapor flow; however, pressure conditions along the structure controlling the upflow of the liquids may be variable during hydrothermal eruptions. As more and more vapor is produced during the onset of the eruption, pressure in the structure drops from hydrostatic to vaporstatic in the upper part of the structure, and the lower pressure regime migrates downward as liquid flashes to vapor at depth and within the surrounding wall rock (Henley and Hughes 2000). As a result, two-phase flow and associated ore deposition may occur over a substantial vertical depth interval, with the nature and permeability of the controlling structure determining to which depth flashing occurs. The maximum depth to which mineralization below the paleosurface is formed is difficult to predict. Ore grade metal enrichment may exist at greater depths in some systems that flashed when compared to systems that simply cooled or perhaps experienced only gentle boiling.

Conclusions

Ore mineral dendrites present in bonanza-type ore samples from four low-sulfidation epithermal deposits were investigated to better constrain the processes of metal enrichment in this deposit type. The ore mineral aggregates have complex multi-branching morphologies and are present in specific types of colloform bands that were originally composed of non-crystalline opal- $A_{\rm G}$ microspheres. The textural evidence suggests that the dendrites grew contemporaneously with the accumulation of the opal- $A_{\rm G}$ microspheres or formed after but within the still permeable, gel-like opal- $A_{\rm G}$ bands. The deposition of the ore mineral dendrites and the silica microspheres can be linked to the occurrence of two-phase flow conditions within the veins following short-lived events of fluid flashing. The observations of this study lend strong support to models emphasizing the importance of

seismically triggered events of flashing in shallow hydrothermal systems as a mechanism for vein formation and ore deposition.

Supplementary Information The online version contains supplementary material available at https://doi.org/10.1007/s00126-023-01187-7.

Acknowledgements We thank James Saunders for help provided during field work at Buckskin National and Fire Creek. John Marma provided a high-grade sample from Fire Creek and James Saunders kindly supported this study by donating sample material from Sleeper. Susann Stolze is thanked for assistance during the HF experiments. We are indebted to Kelsey Livingston for supporting the scanning electron microscopic investigations. Jae Erickson and Sebastian Dettmar are thanked for thin section preparation. We thank an anonymous reviewer and Duncan McLeish for their constructive reviews, which helped us improve an earlier version of the manuscript. Associate editor Matthew Steele-MacInnis is thanked for handling the manuscript.

Author contribution Fieldwork (TT, RS); petrography (ERT, TT, TM, TJR); analytical work (ERT, TT, TM, NMK, KP, ASB); writing (all authors).

Funding This research was partially supported by Equinox Gold through a fellowship to ERT. TT received a Development and Promotion of Science and Technology Talents Project Scholarship from the Royal Thai Government and was awarded the Chevron Research Assistant Fellowship at Colorado School of Mines. A grant by Geological Society of Nevada Elko Chapter to TT supported field work at the Buckskin National and Fire Creek deposits in Nevada.

Declarations

Conflict of interest The authors declare no competing interests.

References

Aseto CO (2012) Geology, geochemistry and geochronology of the mid-Miocene, low-sulfidation epithermal gold-silver ores on War Eagle Mountain, Silver City district, Idaho. Unpublished MS thesis, Auburn University p 170

Bettermann P, Liebau F (1975) The transformation of amorphous silica to crystalline silica under hydrothermal conditions. Contrib Mineral Petrol 53:25–36

Bobis RE (1994) A review of the description, classification and origin of quartz textures in low sulphidation epithermal veins. J Geol Soc Philipp 49:15–39

Bodnar RJ, Lecumberri-Sanchez P, Moncada D, Steele-MacInnis M (2014) Fluid inclusions in hydrothermal ore deposits. In: Holland HD, Turekian KK (eds) Treatise on geochemistry, vol 13. Elsevier, Oxford, pp 119–142

Brenner W, Blank Z, Okamoto Y (1966) Growth of single crystals of lead sulphide in silica gels near ambient temperatures. Nature 212:392–393

Brown KL (1986) Gold deposition from geothermal discharges in New Zealand. Econ Geol 81:979–983

Brown K (2011) Thermodynamics and kinetics of silica scaling. International Workshop on Mineral Scaling, Manila, Philippines, Proceedings, pp 1–8

Burke M, Rakovan J, Krekeler MPS (2017) A study by electron microscopy of gold and associated minerals from Round Mountain, Nevada. Ore Geol Rev 91:708–717



- Campbell KA, Sannazzaro K, Rodgers KA, Herdianita NR, Browne PRL (2001) Sedimentary facies and mineralogy of the late Pleistocene Umukuri silica sinter, Taupo Volcanic Zone, New Zealand. J Sediment Res 71:727–746
- Campbell KA, Rodgers KA, Brotheridge JMA, Browne PRL (2002) An unusual modern silica-carbonate sinter from Pavlova spring, Ngatamariki, New Zealand. Sedimentology 49:835–854
- Chambefort I, Stefánsson A (2020) Fluids in geothermal Systems. Elements 16:407–411
- Christenson BW, Hayba DO (1995) Hydrothermal eruptions in ore forming reservoirs: analogues and models. PACRIM Congress, Exploring the Rim, Auckland, New Zealand. Proceedings, pp 119–124
- Cocker HA, Mauk JL, Rabone SDC (2013) The origin of Ag-Au-S-Se minerals in adularia-sericite epithermal deposits: Constraints from the Broken Hills deposit, Hauraki Goldfield, New Zealand. Miner Deposita 48:249–266
- Conrad JE, McKee EH, Rytuba JJ, Nash JT, Utterback WC (1993) Geochronology of the Sleeper deposit, Humboldt County, Nevada: epithermal gold-silver mineralization following emplacement of a silicic flow-dome complex. Econ Geol 88:317–327
- Dong G, Morrison G, Jaireth S (1995) Quartz textures in epithermal veins, Queensland-Classification, origin, and implication. Econ Geol 90:1841–1856
- Ernst WG, Calvert SE (1969) An experimental study of the recrystallization of porcelanite and its bearing on the origin of some bedded cherts. Am J Sci 267:114–133
- Etoh J, Izawa E, Watanabe K, Taguchi S, Sekine R (2002) Bladed quartz and its relationship to gold mineralization in the Hishikari low-sulfidation epithermal gold deposit, Japan. Econ Geol 97:1841–1851
- Fernandez-Turiel JL, Garcia-Valles M, Gimeno-Torrente D, Saavedra-Alonso J, Martinez-Manent S (2005) The hot spring and geyser sinters of El Tatio, northern Chile. Sediment Geol 180:125–147
- Fisher LW, Simons FL (1926) Applications of colloid chemistry to mineralogy. Part i Preliminary Report. Am Mineral 11:124–130
- Fournier RO, Thompson JM, Cunningham CG, Hutchinson RA (1991) Conditions leading to a recent small hydrothermal explosion at Yellowstone National Park. Geol Soc Amer Bull 103:1114–1120
- Guidry SA, Chafetz HS (2003) Anatomy of siliceous hot springs: examples from Yellowstone National Park, Wyoming, USA. Sediment Geol 157:71–106
- Gustafson DL (1991) Anatomy of a discovery: the McLaughlin gold mine, Napa, Yolo, and Lake counties, California. Econ Geol Monogr 8:350–359
- Halberstadt ES (1967) Growth of single crystals of silver iodide in silica gel. Nature 216:574
- Hawkins C, Angheluta L, Jamtveit B (2014) Hydrodynamic shadowing effect during precipitation of dendrites in channel flow. Phys Rev E 89:022402
- Hedenquist JW, Henley RW (1985) Hydrothermal eruptions in the Waiotapu geothermal system, New Zealand: their origin, associated breccias, and relation to precious metal mineralization. Econ Geol 80:1640–1668
- Hedenquist JW, Arribas A, Gonzalez-Urien E (2000) Exploration for epithermal gold deposits. Rev Econ Geol 13:245–277
- Henley RW, Hughes GO (2000) Underground fumaroles: "excess heat" effects in vein formation. Econ Geol 95:453–466
- Herdianita NR, Browne PRL, Rodgers KA, Campbell KA (2000) Mineralogical and textural changes accompanying ageing of silica sinter. Miner Deposita 35:48–62
- Holmes HN (1917) The formation of crystals in gels. J Franklin Inst 184:743–773
- John DA, Henry CD (2020) Magmatic-tectonic settings of Cenozoic epithermal gold-silver deposits of the Great Basin, western United States. Geol Soc Nevada 2020 Symposium, Geology and

- Ore Deposits of the Basin and Range, Reno-Sparks, Nevada. Proceedings, pp 765–796
- Jones B (2021) Siliceous sinters in thermal spring systems: review of their mineralogy, diagenesis, and fabrics. Sediment Geol 413:105820
- Jones B, Renaut RW, Rosen MR (1997) Biogenicity of silica precipitation around geysers and hot-spring vents, North Island, New Zealand. J Sediment Res 67:88–104
- Keith TEC (1992) A look at silica phases in evolving hydrothermal systems. Proceedings of the 7th International Symposium on Water-Rock Interaction (Park City, Utah), pp 1423–1426
- Kotru PN, Gupta NK, Raina KK (1986) Growth of lanthanum tartrate crystals in silica gel. J Mater Sci 21:90–96
- Krupp RE, Seward TM (1987) The Rotokawa geothermal system, New Zealand: an active epithermal gold-depositing environment. Econ Geol 82:1109–1129
- Leavitt ED, Spell TL, Goldstrand PM, Arehart GB (2004) Geochronology of the Midas low-sulfidation epithermal gold-silver deposit, Elko County, Nevada. Econ Geol 99:1665–1686
- Lindgren W (1915) Geology and mineral deposits of the National Mining district, Nevada. U.S. Geol Surv Bull 601:58 p
- Lindgren W (1936) Succession of minerals and temperatures of formation in ore deposits of magmatic affiliations. Am Inst Mining Metall Eng Techn Publ p 713:23
- Lovering TG (1972) Jasperoid in the United States: its characteristics, origin, and economic significance. U.S. Geol Surv Bull p 710:164
- Lynne BY, Campbell KA (2004) Morphologic and mineralogic transitions from opal-A to opal-CT in low-temperature siliceous sinter diagenesis, Taupo Volcanic Zone, New Zealand. J Sediment Res 74:561–579
- Lynne BY, Campbell KA, Moore JN, Browne PRL (2005) Diagenesis of 1900-year-old siliceous sinter (opal-A to quartz) at Opal Mound, Roosevelt Hot Springs, Utah, U.S.A. Sediment Geol 179:249–278
- Lynne BY, Campbell KA, James BJ, Browne PRL, Moore J (2007) Tracking crystallinity in siliceous hot-spring deposits. Am J Sci 307:612–641
- Marini L, Principe C, Chiodini G, Cioni R, Fytikas M, Marinelli G (1993) Hydrothermal eruptions of Nisyros (Dodecanese, Greece). Past events and present hazard. J Volcanol Geoth Res 56:71–94
- Marinova I, Ganev V, Titorenkova R (2014) Colloidal origin of colloform-banded textures in the Paleogene low-sulfidation Khan Krum gold deposit, SE Bulgaria. Miner Deposita 49:49–74
- Mason MS, Saunders JA, Aseto C, Hames WE (2015) Epithermal Au-Ag ores of War Eagle and Florida Mountains, Silver City district, Owyhee County, Idaho. Geol Soc Nevada Symposium, New Concepts and Discoveries, Reno, Nevada. Proceedings pp 859–870
- McCauley JW, Roy R (1974) Controlled nucleation and crystal growth of various ${\rm CaCO_3}$ phases by the silica gel technique. Am Mineral 59:947–963
- Meier DB, Gunnlaugsson E, Gunnarsson I, Jamtveit B, Peacock CL, Benning LG (2014) Microstructural and chemical variation in silica-rich precipitates at the Hellisheiði geothermal power plant. Mineral Mag 78:1381–1389
- Milliard JB, Marma JC, Kassos G, Hobbs E, Borchardt JS, Rehak KR (2015) Geology of the Fire Creek exploration project—low-sulfidation epithermal bonanza gold-silver deposit, Lander County, Nevada, USA. Geol Soc Nevada Symposium, New Concepts and Discoveries, Reno, Nevada. Proceedings pp 1339–1364
- Moncada D, Mutchler S, Nieto A, Reynolds TJ, Rimstidt JD, Bodnar RJ (2012) Mineral textures and fluid inclusion petrography of the epithermal Ag–Au deposits at Guanajuato, Mexico: application to exploration. J Geochem Explor 114:20–35



- Monecke T, Reynolds TJ, Taksavasu T, Tharalson ER, Zeeck LR, Guzman M, Gissler G, Sherlock R (2023) Natural growth of gold dendrites within silica gels. Geology 51:189–192
- Mroczek E, Graham D, Siega C, Bacon L (2017) Silica scaling in cooled silica saturated geothermal water: comparison between Wairakei and Ohaaki geothermal fields, New Zealand. Geothermics 69:145–152
- Muffler LJP, White DE, Truesdell AH (1971) Hydrothermal explosion craters in Yellowstone National Park. Geol Soc Am Bull 82:723–740
- Muzikář M, Komanický V, Fawcett WR (2006) A detailed study of gold single crystal growth in a silica gel. J Cryst Growth 290:615-620
- Nairn IA, Wiradiradja S (1980) Late Quaternary hydrothermal explosion breccias at Kawerau geothermal field, New Zealand. Bull Volcanol 43:1–13
- Nash JT, Utterback WC, Saunders JA (1989) Geology and geochemistry of the Sleeper gold-silver deposit, Humboldt County, Nevada—an interim report. U.S. Geol Surv Open-File Rep 39:89–476
- Nash JT, Utterback WC, Trudel WS (1995) Geology and geochemistry of Tertiary volcanic host rocks, Sleeper gold-silver deposit, Humboldt County, Nevada. U.S. Geol Surv Bull 2090 p 63
- Oaki Y, Imai H (2003) Experimental demonstration for the morphological evolution of crystals grown in gel media. Cryst Growth Des 3:711–716
- Odell M, Symmes L, Bull S, Knight A (2018) Technical report for the Fire Creek project, Lander County, Nevada. Practical Mining LLC p 269
- Oehler JH (1976) Hydrothermal crystallization of silica gel. Geol Soc Am Bull 87:1143–1152
- Perez J (2013) Origin of basalt-hosted epithermal gold-silver mineralization in the Fire Creek deposit, northern Nevada Rift from a whole-rock to grain-scale perspective. Unpublished MS thesis, University of California, p 107
- Raj AME, Jayanthi DD, Jothy VB (2008) Optimized growth and characterization of cadmium oxalate single crystals in silica gel. Solid State Sci 10:557–562
- Raymond J, Williams-Jones AE, Clark JR (2005) Mineralization associated with scale and altered rock and pipe fragments from the Berlín geothermal field, El Salvador: implications for metal transport in natural systems. J Volcanol Geoth Res 145:81–96
- Reyes AG, Trompetter WJ, Britten K, Searle J (2002) Mineral deposits in the Rotokawa geothermal pipelines, New Zealand. J Volcanol Geoth Res 119:215–239
- Rodgers KA, Browne PRL, Buddle TF, Cook KL, Greatrex RA, Hampton WA, Herdianita NR, Holland GR, Lynne BY, Martin R, Newton Z, Pastars D, Sannazarro KL, Teece CIA (2004) Silica phases in sinters and residues from geothermal fields of New Zealand. Earth-Sci Rev 66:1–61
- Rothbaum HP, Anderton BH, Harrison RF, Rohde AG, Slatter A (1979) Effect of silica polymerisation and pH on geothermal scaling. Geothermics 8:1–20
- Rowland JV, Simmons SF (2012) Hydrologic, magmatic, and tectonic controls on hydrothermal flow, Taupo Volcanic Zone, New Zealand: implications for the formation of epithermal vein deposits. Econ Geol 107:427–457
- Sanematsu K, Watanabe K, Duncan RA, Izawa E (2006) The history of vein formation determined by ⁴⁰Ar/³⁹Ar dating of adularia in the Hosen-1 vein at the Hishikari epithermal gold deposit, Japan. Econ Geol 101:685–698
- Saunders J (1990) Colloidal transport of gold and silica in epithermal precious-metal systems: evidence from the Sleeper deposit, Nevada. Geology 18:757–760
- Saunders JA (1994) Silica and gold textures in bonanza ores of the Sleeper deposit, Humboldt County, Nevada: evidence for colloids

- and implications for epithermal ore-forming processes. Econ Geol 89:628–638
- Saunders JA (2012) Textural evidence of episodic introduction of metallic nanoparticles into bonanza epithermal ores. Minerals 2:228–243
- Saunders JA, Burke M (2017) Formation and aggregation of gold (electrum) nanoparticles in epithermal ores. Minerals 7:163
- Saunders JA, Schoenly PA (1995a) Fractal structure of electrum dendrites in bonanza epithermal Au-Ag deposits. In: Barton CC, La Pointe PR (eds) Fractals in the earth sciences. Springer, New York, pp 251–261
- Saunders JA, Schoenly PA (1995b) Boiling, colloid nucleation and aggregation, and the genesis of bonanza Au-Ag ores of the Sleeper deposit, Nevada. Miner Deposita 30:199–210
- Saunders JA, Unger DL, Kamenov GD, Fayek M, Hames WE, Utterback WC (2008) Genesis of middle Miocene Yellowstone hotspot-related bonanza epithermal Au–Ag deposits, northern Great Basin, USA. Miner Deposita 43:715–734
- Saunders JA, Burke M, Brueseke ME (2020) Scanning-electronmicroscope imaging of gold (electrum) nanoparticles in middle Miocene bonanza epithermal ores from northern Nevada, USA. Miner Deposita 55:389–398
- Saunders JA, Cook RB, Schoenly PA (1996) Electrum disequilibrium crystallization textures in volcanic-hosted bonanza epithermal gold deposits. Geol Soc Nevada, Geology and Ore Deposits of the American Cordillera Symposium, Reno-Sparks. Proceedings pp 173–179
- Saunders JA, Vikre P, Unger DL, Beasley L (2011) Colloidal and physical transport textures exhibited by electrum and naumannite in bonanza epithermal veins from western USA, and their significance. Geol Soc Nevada, Great Basin Evolution and Metallogeny Symposium, Reno-Sparks, Nevada. Proceedings pp 825–832
- Schinteie R, Campbell KA, Browne PRL (2007) Microfacies of stromatolitic sinter from acid-sulphate-chloride springs at Parariki Stream, Rotokawa geothermal field, New Zealand. Palaeontologia Electronica 10:33
- Sherlock RL, Lehrman NJ (1995) Occurrences of dendritic gold at the McLaughlin mine hot-spring gold deposit. Miner Deposita 30:323–327
- Sherlock RL, Tosdal RM, Lehrman NJ, Graney JR, Losh S, Jowett EC, Kesler SE (1995) Origin of the McLaughlin mine sheeted vein complex: metal zoning, fluid inclusion, and isotopic evidence. Econ Geol 90:2156–2181
- Shimizu T (2014) Reinterpretation of quartz textures in terms of hydrothermal fluid evolution at the Koryu Au-Ag deposit, Japan. Econ Geol 109:2051–2065
- Shimizu T, Matsueda H, Ishiyama D, Matsubaya O (1998) Genesis of epithermal Au-Ag mineralization of the Koryu Mine, Hokkaido, Japan. Econ Geol 93:303–325
- Simmons SF, Brown KL (2007) The flux of gold and related metals through a volcanic arc, Taupo Volcanic Zone, New Zealand. Geology 35:1099–1102
- Simmons SF, Browne PRL (2000) Hydrothermal minerals and precious metals in the Broadlands-Ohaaki geothermal system: implications for understanding low-sulfidation epithermal environments. Econ Geol 95:971–999
- Simmons SF, White NC, John DA (2005) Geological characteristics of epithermal precious and base metal deposits. In: Hedenquist JW, Thompson JFH, Goldfarb RJ, Richards JP (eds) Economic Geology 100th Anniversary Volume, pp 485–522
- Simpson M (2017) Microthermometry of deep veins from the Waihi, Karangahake and Tui epithermal vein deposits, southern Hauraki Goldfield. Proceedings of the Australasian Institute of Mining and Metallurgy 49th New Zealand Branch Annual Conference, Christchurch, New Zealand, September 2016, Proceedings, pp 284–293



- Smith DK (1998) Opal, cristobalite, and tridymite: Noncrystallinity versus crystallinity, nomenclature of the silica minerals and bibliography. Powder Diffraction 13:2–19
- Takeuchi K, Shikazono N (1984) Mineralization of the Arakawa No. 4 vein of the Kushikino mine, Kagoshima Prefecture. Japan Mining Geol 34:187–195
- Taksavasu T, Monecke T, Reynolds TJ (2018) Textural characteristics of non-crystalline silica in sinters and quartz veins: implications for the formation of bonanza veins in low-sulfidation epithermal deposits. Minerals 8:331
- Tharalson ER, Monecke T, Reynolds TJ, Zeeck L, Pfaff K, Kelly N (2019) The distribution of precious metals in high-grade banded quartz veins from low-sulfidation epithermal deposits: constraints from μXRF mapping. Minerals 9:740
- Tosdal RM, Sherlock RL, Nelson GC, Enderlin DA, Lehman NJ (1996) Precious metal mineralization in a fold and thrust belt: the McLaughlin hot spring deposit, northern California. Geol Soc Nevada, Geology and Ore Deposits of the American Cordillera Symposium, Reno-Sparks, Nevada. Proceedings, pp 839–854
- Unger DL (2008) Geochronology and geochemistry of mid-Miocene bonanza low-sulfidation epithermal ores of the northern Great Basin, USA. Unpublished MS thesis, Auburn University, p 133
- van den Heuvel DB, Gunnlaugsson E, Gunnarsson I, Stawski TM, Peacock CL, Benning LG (2018) Understanding amorphous silica scaling under well-constrained conditions inside geothermal pipelines. Geothermics 76:231–241
- Vikre PG (1985) Precious metal vein systems in the National District, Humboldt County, Nevada. Econ Geol 80:360–393
- Vikre PG (1987) Paleohydrology of Buckskin Mountain, National district, Humboldt County, Nevada. Econ Geol 82:934–950
- Vikre PG (2007) Sinter-vein correlations at Buckskin Mountain, National district, Humboldt County, Nevada. Econ Geol 102:193–224

- Weissberg BG (1969) Gold-silver ore-grade precipitates from New Zealand thermal waters. Econ Geol 64:95–108
- Wilson SE, Brechtel C (2017) Technical report and preliminary economic assessment Paramount Gold Nevada Corp. Sleeper project, Humboldt County, Nevada. Metal Mining Consultants Inc. p 215
- Wood JD, Hamilton SK (1991) The Sleeper gold-silver deposit: discovery through feasibility. Econ Geol Monogr 8:289–299
- Zarrouk SJ, Woodhurst BC, Morris C (2014) Silica scaling in geothermal heat exchangers and its impact on pressure drop and performance: Wairakei binary plant, New Zealand. Geothermics 51:445–459
- Zeeck LR, Monecke T, Reynolds TJ, Tharalson ER, Pfaff K, Kelly NM, Hennigh Q (2021) Textural characteristics of barren and mineralized colloform quartz bands at the low-sulfidation epithermal deposits of the Omu Camp in Hokkaido, Japan: Implications for processes resulting in bonanza-grade precious metal enrichment. Econ Geol 116:407–425

Publisher's note Springer Nature remains neutral with regard to jurisdictional claims in published maps and institutional affiliations.

Springer Nature or its licensor (e.g. a society or other partner) holds exclusive rights to this article under a publishing agreement with the author(s) or other rightsholder(s); author self-archiving of the accepted manuscript version of this article is solely governed by the terms of such publishing agreement and applicable law.

